SURFACE ENHANCED RAMAN SCATTERING WITH GOLD NANOSTAR AND QUANTUM DOT HYBRID STRUCTURES

A THESIS SUBMITTED TO
THE GRADUATE SCHOOL OF NATURAL AND APPLIED SCIENCES
OF
MIDDLE EAST TECHNICAL UNIVERSITY

BY

DUYGU GÜMÜŞ

IN PARTIAL FULFILLMENT OF THE REQUIREMENTS
FOR
THE DEGREE OF MASTER OF SCIENCE
IN
CHEMISTRY

FEBRUARY 2023

Approval of the thesis:

SURFACE ENHANCED RAMAN SCATTERING WITH GOLD NANOSTAR AND QUANTUM DOT HYBRID STRUCTURES

submitted by **DUYGU GÜMÜŞ** in partial fulfillment of the requirements for the degree of **Master of Science** i**n Chemistry, Middle East Technical University** by,

Prof. Dr. Halil Kalıpçılar
Dean, Graduate School of **Natural and Applied Sciences** _____

Prof. Dr. Özdemir Doğan
Head of the Department, **Chemistry Department, METU** _____

Prof. Dr. Emren Nalbant
Supervisor, **Chemistry Department, METU** _____

Examining Committee Members:

Prof. Dr. Ayşen Yılmaz
Chemistry Dept., METU _____

Prof. Dr. Emren Nalbant
Chemistry Dept., METU _____

Prof. Dr. Alpan Bek
Physics Dept., METU _____

Prof. Dr. Ali Çırpan
Chemistry Dept., METU _____

Prof. Dr. Murat Kaya
Chemical Eng., Atılım University _____

Date: 24.02.2023

I hereby declare that all information in this document has been obtained and presented in accordance with academic rules and ethical conduct. I also declare that, as required by these rules and conduct, I have fully cited and referenced all material and results that are not original to this work.

Name Last name : Duygu Gümüş

Signature :

ABSTRACT

SURFACE ENHANCED RAMAN SCATTERING WITH GOLD NANOSTAR AND QUANTUM DOT HYBRID STRUCTURES

Gümüş, Duygu
Master of Science, Chemistry
Supervisor: Prof. Dr. Emren Nalbant

February 2023, 60 pages

Noble metal nanoparticles (NMNPs) are an area of increasing interest and active research, due to their distinctive optical and electrical properties which are related to localized surface plasmon resonance. In particular, gold nanoparticles (AuNPs) have become focus of intense research due to their superior optical properties among all noble metal nanoparticles. These properties lead them to be used in wide areas of application like imaging, delivery carriers, chemical sensing and optoelectronic devices. Similar to Au NPs, quantum dots (QDs), too, are attracting well deserved attention owing to their enhanced optical and electrical properties like high photoluminescence (PL), photostability and extinction coefficient.

Different type of nanomaterials and their combinations are used as a substrate for surface-enhanced Raman spectroscopy (SERS) to aid identification of target analyte. However, to the best of our knowledge, Au nanostars and QDs hybrid structure have not used as a SERS substrate, yet.

In this study, star-shaped AuNPs have been synthesized by a seed-mediated growth method. Cadmium Selenide/Zinc Sulfide (CdSe/ZnS) core/shell type quantum dots (QDs) were mixed with star shaped AuNPs in various amounts to observe physical adsorption between QDs and AuNPs. The structure and spectroscopic properties of mixture of QDs and AuNPs were characterized by a combination of UV-Vis spectroscopy, and focused ion beam (FIB). This research demonstrated the potential of this technique to allow controlled signal enhancement of Raman spectroscopy through surface enhanced Raman scattering (SERS).

Keywords: Gold nanoparticles, Surface enhanced Raman scattering, Quantum dots

ÖZ

ALTIN NANOYILDIZ VE KUANTUM NOKTA HİBRİT YAPILARI İLE YÜZEY GELİŞTİRİLMİŞ RAMAN SAÇILMASI

Gümüş, Duygu
Yüksek Lisans, Kimya
Tez Yöneticisi: Prof. Dr. Emren Nalbant

Şubat 2023, 60 sayfa

Soy metal nanopartiküller lokalize yüzey plazmon rezonansı ile ilgili ayırt edici optik ve elektriksel özelliklerinden dolayı artan bir ilgi ve aktif araştırma alanıdır. Özellikle altın nanopartiküller (AuNP'ler), tüm soy metal nanopartiküller arasında üstün optik özelliklerinden dolayı yoğun araştırmaların odağı haline gelmiştir. Bu özellikleri, görüntüleme, dağıtım taşıyıcıları, kimyasal algılama ve optoelektronik cihazlar gibi geniş uygulama alanlarında kullanılmalarına yol açar. AuNP'lere benzer şekilde, kuantum noktaları da yüksek fotolüminesans, fotostabilite ve sönüm katsayısı gibi gelişmiş optik ve elektriksel özellikleri sayesinde popüler bir çalışma konusu haline gelmiştir. Farklı türde nanomalzemeler ve bunların kombinasyonları, hedef analitin tanımlanmasına yardımcı olmak için yüzeyi geliştirilmiş Raman spektroskopisi için bir substrat olarak kullanılır. Ancak, bildiğimiz kadarıyla, altın nanoyıldız ve kuantum noktalar hibrit yapısı henüz bir yüzeyi geliştirilmiş Raman spektroskopisi substratı olarak kullanılmamıştır. Bu çalışmada, yıldız şeklindeki AuNPler, tohum aracılı bir büyüme yöntemiyle sentezlendi. Kadmiyum Selenit/Çinko Sülfür (CdSe/ZnS) çekirdek/kabuk tipi kuantum noktaları ve AuNP'ler arasındaki fiziksel adsorpsiyonu gözlemlemek için yıldız şeklindeki AuNPlerle çeşitli miktarlarda karıştırıldı. Kuantum noktaların ve AuNP'lerin

karışımının yapısı ve spektroskopik özellikleri, UV-Vis spektroskopisi ve odaklanmış iyon demeti kombinasyonu ile karakterize edildi. Bu araştırma, yüzey geliştirilmiş Raman saçılması yoluyla Raman spektroskopisinin kontrollü sinyal geliştirmesine izin vermek için bu tekniğin potansiyelini göstermiştir.

Anahtar Kelimeler: Altın nanoparçacıklar, Yüzeyde güçlendirilmiş Raman spektroskopisi, Kuantum noktaları

To my lovely parents and beautiful sisters…

ACKNOWLEDGMENTS

I would like to thank my teacher Prof. Dr. Emren NALBANT, who is one of my greatest lucky breaks at this university, a thousand times. She always trusted me and encouraged me every time I said I couldn't do it.

A lot of thanks to Prof. Alpan Bek and Özge Demirtaş for their assistance. I couldn´t do without Özge´s guidance and patience. She deserves the best for everything.

My second chance during my Master´s degree, to my friends Almila and Firdevs, for their unquestioning support and love. That means a lot for me during my journey. My group members, Aleyna, Mete, Başak, and Ecem for their great company. To Doğan, his endless patience and support for me.

My family, who are my biggest chance in my life. If I am a successful and independent woman right now, it's all thanks to them. I love you more than anything, my dear father Olgun, adoring mother Sevgi, and my two beautiful sisters, Bilge and Özge.

Petter Torvund Lund, you are the biggest motivation for all my efforts. Thank you for keeping my ambitions and goals high.

This work is funded by Scientific and Technological Research Council of Turkey under grant number TUBİTAK 119F101.

TABLE OF CONTENTS

TABLE OF FIGURES

FIGURES

CHAPTER 1

INTRODUCTION

1.1. Motivation for Study

Nanoparticles, are an ever-increasing field of study with many different application areas due to their unique optical and chemical properties. Gold nanoparticles (AuNPs) are one of the well-known nanoparticles due to their low toxicity, stability, and optical properties. In particular, the tunable optical properties of AuNPs, which vary with the size and shape of the particle, and surface plasmon resonance (SPR) activity that can be induced, makes AuNPs an interesting platform for a number of application areas.[1] One key area of research is surface enhanced Raman scattering (SERS) due to SPR property of AuNPs. According to electromagnetic enhancement mechanism of SERS, additional electromagnetic fields emerge, enhancing the Raman signals.[2] This makes AuNPs preferable substrates for SERS. In the existing literature there are several threads of research about SERS with AuNPs. Substrates of SERS may not only be simple AuNPs but also modified form of AuNPs like coated, alloy and core-shell nanostructures.[3,4,5]

Similar to Au NPs, quantum dots (QDs) are also popular materials for applications where special optical properties are needed. QDs are semiconductor nanostructures which have different electronic and optical features from their bulk form. In particular their broad absorption and narrow emission bands make QDs a material of interest in application areas such as solar cells, light emitting diode (LED) and laser sources.[6,7,8]

Pairs of AuNPs are able to produce hot spots areas where enhancement of light-matter interaction occurs. When QDs are placed at these hot spots, they interact strongly with the localized plasmon field. This interaction enables rising nonlinear processes like second harmonic generation (SHG), SERS and four wave mixing (FWM). In double plasmon mode systems, these nonlinear processes are even more pronounced when the frequencies of the converted electromagnetic field are equal to the frequency of the plasmon mode. [9,10]

SERS amplification with Fano resonances (FR) in the literature relies on increasing hot spot intensity by selecting stimulus (e.g. 593 nm) and Stokes signal (e.g. 700 nm) wavelengths which coincide with the two Fano resonances.[11,12] This has the effect of extending plasmon lifetimes which, while it does provide signal enhancement, can damage the molecule imaged with SERS or modification of vibration modes. At the same time, due to quantum tunneling, the field strength is ultimately limited by SERS signal amplification.[13,70]

To overcome these barriers, this research set out to provide an experimental demonstration of an approach to overcome current quantum tunneling limit and eliminate the molecular vibration modes excitation/modification problem. This proposed approach which is called as silent enhancement of SERS

would therefore allow a significant increase in the efficiency of SERS imaging in both high-intensity field localization and quantum tunneling limits.[70]

In literature, different types of nanomaterials like AuNPs, silver (Ag) NPs and QDs are used as a SERS substrate to observe the enhancement.[14,15] Additionally, studies on combinations of different NPs, coating of nanomaterials and their hybrid structures can be found in the literature.[16,17] For instance, a study by Du et al [18] reported that SERS enhancement factor was up to 10^7 with a graphene-Au hybrid structure for SERS detection of rhodamine-6G (R6G). Also, another study by Fang et al [19] shows that SERS enhancement factor of gold-core–palladium-shell nanoparticles is calculated as $5x10^4$ which is higher than pure Pd electrode in pyridine detection. However, number of studies using combination of AuNPs and

QDs as SERS substrate is scarce. To the best of our knowledge only one study has been reported on such hybrid material as a PhD dissertation to date. In this reported study,[20] Cadmium Selenide/Zinc Sulfide (CdSe/ZnS) core-shell type QDs and popcorn shaped AuNPs (PS-AuNPs) were functionalized by ligand exchange reaction and 4-mercapobenzoic acid (4-MBA) was used as a probe molecule. Conjugated system of PS-AuNPs and QDs enhanced the electromagnetic field 10 times stronger than PS-AuNPs for 4-MBA. This study showed that QDs and AuNPs hybrid structures have a potential to be used as a SERS substrate.

In this study, hybrid structure of CdSe/ZnS QD and Au nanostar was used as a SERS substrate. Star shaped AuNPs were specifically selected for their superior performance in SERS as noted in various study reported in the literature.[21,22,23] CdSe/ZnS core-shell quantum dots were preferred in this study due to their size, high extinction coefficient, high photostability and high photoluminescence quantum yield (PLQY). The main idea behind using this hybrid structure is that neither the Raman excitation wavelength, the QDs energy level range, nor the evolved (Stokes) signal wavelength match the plasmon modes wavelength, thereby there will be no change in hotspot intensity and silent enhancement of SERS will be responsible enhancing the Raman signal of target molecule. In light of the literature presented above a QD and AuNP hybrid structure is used in SERS to enhance the signal of target molecule.

1.2. Nanoparticles

Nanotechnology refers to the study and application of particles at the nanoscale, which are bigger than individual atoms but much smaller than daily objects (i.e., 1 m= 10^{-9} nm) and common macromolecules. Sizes of nanoparticles are generally between 1 and 100 nm. When the particle size decreases to nanoscale, properties of material changes dramatically compared to the bulk form of the material, especially for metal nanoparticles. Metal nanoparticles have lower melting points, special optical properties and different mechanical strengths compared to bulk metal

materials. These novel properties of metal nanoparticles have opened a new field of scientific research with industrial applications like sensing, catalysis, drug delivery in medicine etc. [24,25,26]

1.3. Gold Nanoparticles

AuNPs are in the limelight as a result of their unique optoelectronic properties, biocompatibility and low toxicity.[27] Compared to bulk gold, AuNPs have a higher surface area to volume ratio which enables AuNPs to appear a variety of colors (including purple, blue and red) compared to the simple yellow of bulk gold. These colors are a result of the confinement of localized surface plasmon resonance (LSPR) to a small surface. The wavelengths which interact with the nanoparticles is between 400 nm and 700 nm (within the spectrum of visible light) are much larger than the size of the nanoparticles themselves.[28] Electron clouds in the material are excited by this external wavelength, resulting in distortion of electron clouds. Strong absorption occurs when the oscillation of localized surface plasmon resonates with the oscillation of light. LSRP vary with the specific size, shape, dielectric constant of the medium and quality of the carrier liquid.[29] Figure 1.1 represents formation of the LSRP.

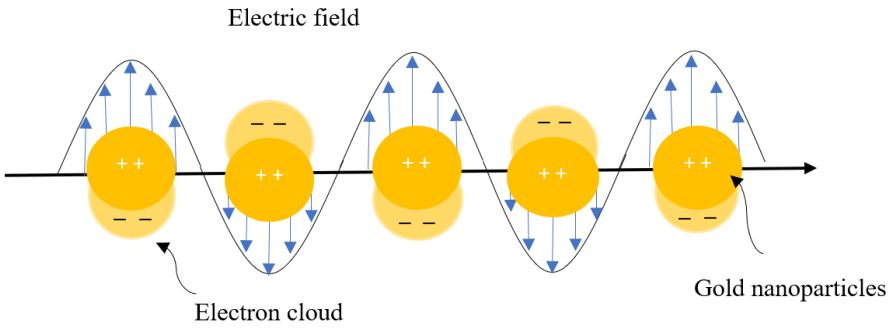

Figure 1.1. Formation of surface resonance plasmon.[30]

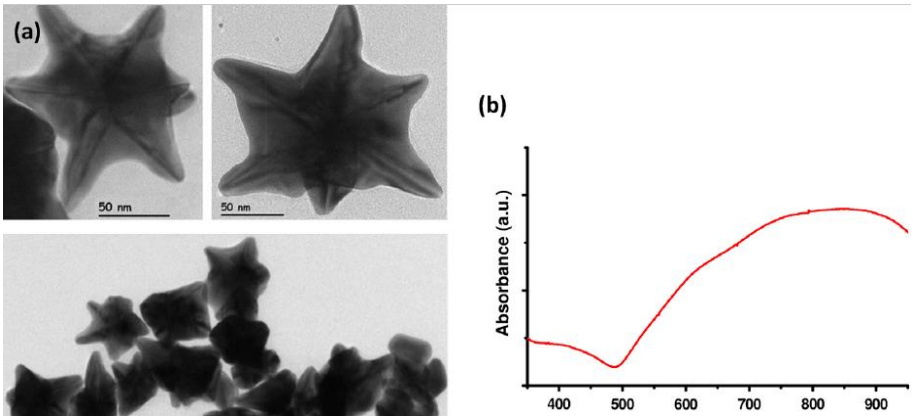

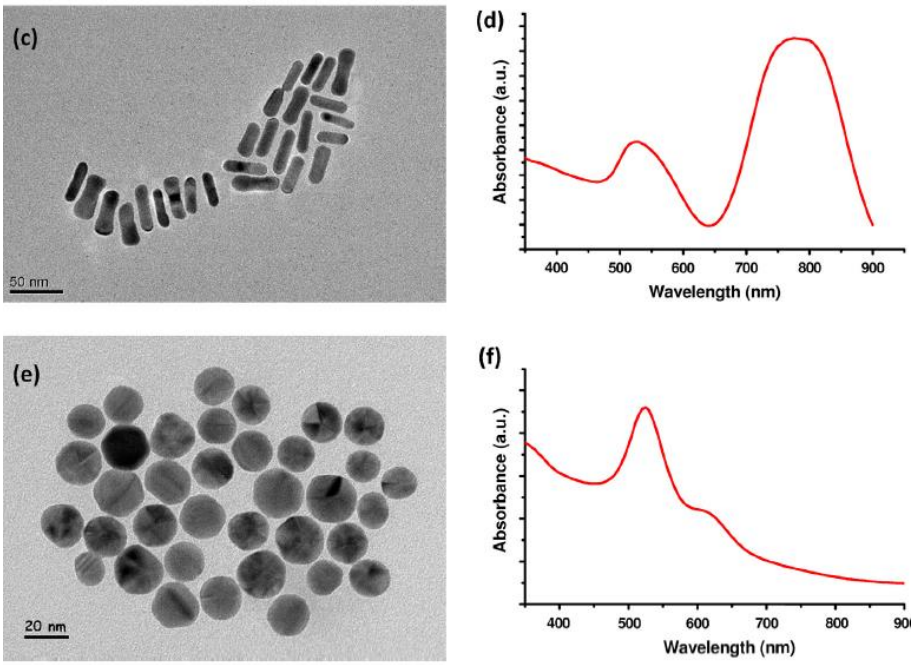

Figure 1.2. TEM image of Au (a) nanostars, (b) nanorods, (c) nanospheres, and UV–vis absorption spectrum of (a) nanostar, (b) nanorod, and (c) nanosphere colloids in aqueous medium. [23]

Transmission Electron Microscopy (TEM) images and absorption spectrum of three different gold particles are given in Figure 1.2. While spherical (c) and cylindrical shapes of nanorods (b) absorb light around 550 nm and 720 nm respectively, sharp, and blunt tips of nanostars (a) absorb a wider spectrum of wavelengths. This clearly shows that shape of AuNPs plays an important role in optical properties.

1.4. Synthesis of gold nanoparticles

Knowing that the shape and size of the AuNPs play important roles in application, this leads to the need to investigate distinct synthesis methods for AuNPs. Bottom-up and top-down are two approaches to synthesize AuNPs as well as synthesizing noble metal nanoparticles. The top-down method aims to break bulk materials into nano scale particles progressively using mechanical processing. This method has

some drawbacks, like broad size distribution and high cost.[31] In the bottom-up approach chemical reactions among the atoms/ions/molecules under certain conditions combine small particles to build larger nanoparticles. [32] The bottom-up approach is the more common technique used to synthesize AuNPs due to its affordability, versatility, and ease of application.[33]

1.4.1. Electrochemical method

The electrochemical method was first investigated by Reetz and Helbig in 1994 to synthesize metal nanoparticles. The basis of this method is on the use of the bulk form of metal as an anode, resulting in nanoparticle formation. Metal is oxidized at the anode and after oxidation metal cations are passed through the cathode. In the cathode metal cations are reduced to the zero-oxidation state. Agglomeration of these colloidal metal clusters is prevented by virtue of the supporting electrode, which is made of a stabilizer material like tetraoctylammonium bromide (TOAB). This study also showed that particle size can be controlled by current density.[34]

Further research has elaborated on the effect of synthesis parameters like growth temperature, current density, and amount of surfactant on AuNP particle size. [35]

1.4.2. Turkevich Method

Turkevich pioneered the synthesis of AuNPs through a novel method, based on reduction of gold ions (Au^{3+}) to gold atoms (Au^{0}) by reducing agents and followed by stabilizing the present AuNPs through the addition of a capping/stabilizing agent. In the Turkevich method citrate ions act as both reducing and stabilizing agent. The size of the AuNPs which are synthesized by the Turkevich method is between 10 nm-20 nm.[36,37]

The narrow size range was a limitation of the original Turkevich method leading researchers to attempt to expand the size range of AuNPs. In 1973, Frens

successfully synthesized AuNPs within the range of 15 nm-147 nm by altering the ratio of reducing agent to stabilizing agent, demonstrating the broader relevance of the Turkevich method.[38, 39 ,40]

1.4.3. Brust-Schiffrin Method

In 1994, Brust and Schiffrin discovered a new way to synthesize AuNPs via a two-phase liquid-liquid system. By using tetraoctylammonium (TOAB) as the interfacial carrier, gold ions are transferred to the toluene phase from the aqueous phase. Reduction of Au^{3+} ions is achieved with the use of sodium borohydride as a reducing agent. The formed nanoparticles were then stabilized using a mixture of thiols. One of the advantages of using this method is that the resulting stable AuNPs with narrow size distribution (1-3 nm) can be synthesized in a common organic solvent. [41,42]

1.4.4. Seed-Mediated Growth Method

Seed-mediated growth methods are based on a two-step process of nucleation and growth. In the nucleation step, initial nanocrystals (known as seeds) are formed. In the second step, the growth solution is added, which triggers the production of more nanoparticles from the seed crystals formed in the first step. During these two steps, stabilizing, reducing, and shape directing agents are commonly used to synthesize AuNPs. The main role of a stabilizing (capping) agent is to prevent uncontrollable growth and aggregation. By using capping agents, particle size can be controlled and tuned. There are two types of stabilization which are electrostatic and steric stabilization. In steric stabilization, polymers or surfactants are adsorbed by nanoparticles and create a physical barrier to prevent agglomeration.[43] Repulsive electrostatic double-layer forces are the underlying mechanism of electrostatic stabilization. Metal particles give partial positive charge on the surface and are surrounded by negatively charged particles which creates repulsive forces between two metal nanoparticles.[44,45]

One of the well-known shape of nanoparticles which are synthesized with this method is nanorods. In figure 1.3 basic steps of seed-mediated method are shown.

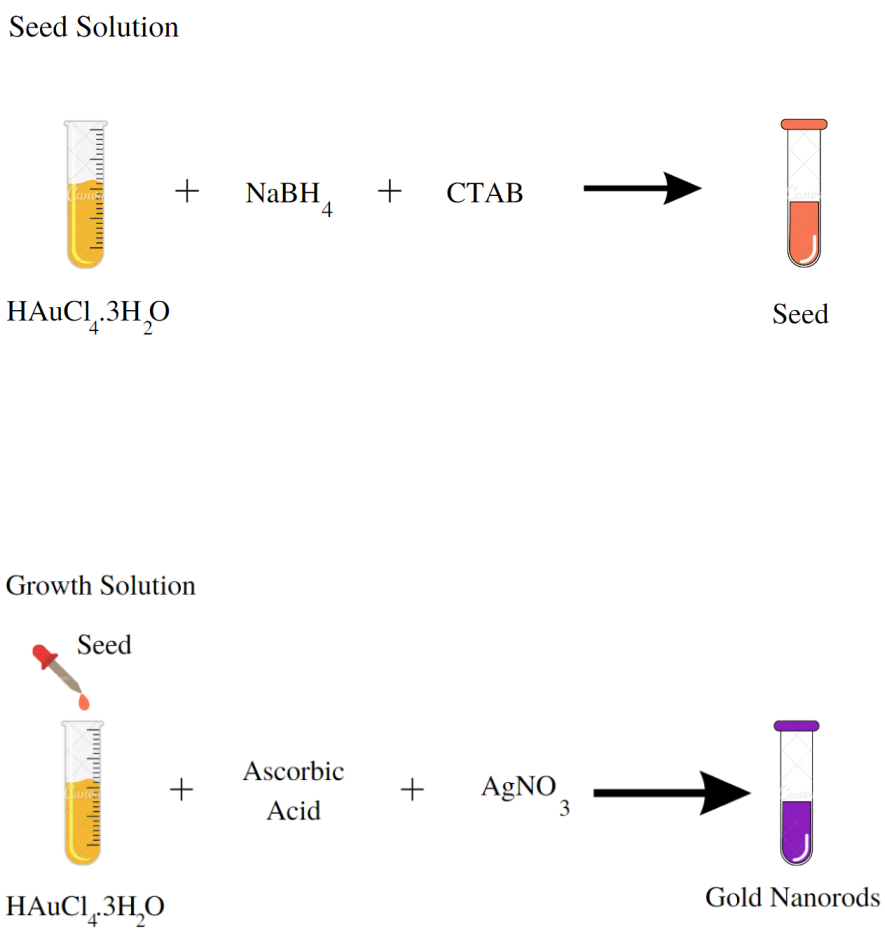

Figure 1.3. Steps in synthesis of gold nanorods.

Metal salt, $HAuCl_4$, is reduced by strong reducing agent which is $NaBH_4$ in presence of capping agent like cetyltrimethylammonium bromide (CTAB). At the end of this step seed crystals are formed. Seeds are added to growth solution which contains metal salt, weak reducing agent (i.e. ascorbic acid) and CTAB as a capping agent. Seed crystals then trigger the formation of further nanoparticles in the growth

solution. Shape of AuNPs is directed by silver nitrate ($AgNO_3$) as shape directing agent. [46,47]

1.5. Surface-Enhanced Raman Scattering Spectroscopy

Interaction of the sample with the light source results in absorption, transmission, reflection and scattering of the light. When the energy of incident light does not match with any energy separation of the molecule, this results in transmission or scattering. This is normally a rare event which involves only a small fraction of the incoming photons. In most cases, the initial frequency is equal to the final frequency of scattered light, in other words there is no chance in energy; this is known as Rayleigh scattering which is an elastic type of scattering. About 99.9% of the scattering is Rayleigh scattering, however around 0.1% scattering results in changing the initial energy. If the emission frequency is lower than initial frequency, it is called Stokes scattering. On the other hand, higher emission values indicate anti-Stokes scattering. Both anti-Stoke and Stokes shifts are sign of the change in initial energy. The difference between the initial and final energy gives information about the vibrational frequency of the molecule. Different molecules vibrate at distinct frequencies, so these vibrational frequencies are specific to the molecule. With the help of Raman scattering, qualitative analyses can be done by checking the Raman shifts, on the other hand intensity of the Raman bands are the key for quantitative analyses. Figure 1.4. represents the schematic diagram of Rayleigh and Raman scattering. [48,49]

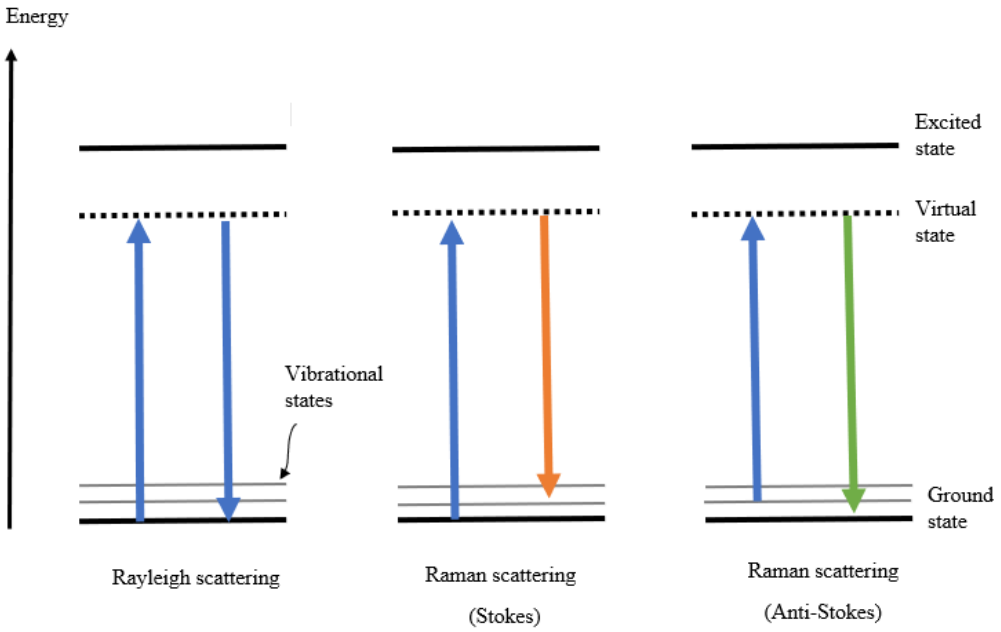

Figure 1.4. Schematic diagram of Rayleigh and Raman scattering.[50]

Fast characterization, no sample preparation requirement and portability are some of the advantages of Raman spectroscopy.[51] Although Raman spectroscopy has some advantages, it also has limitations like all methodologies. About 1 in 10^7 incident photons is Raman scattered, resulting in a very low signal intensity which is the main drawback of this approach.[52] SERS spectroscopy is a technique developed to overcome this traditional limitation of classical Raman spectroscopy in order to increase the magnitude of the Raman signal.[53]

The mechanism of SERS is still under investigation. There are several proposed mechanisms to SERS however chemical enhancement theory (CE) and electromagnetic enhancement theory (EME) are two widely recognized and accepted proposed theories. EME is associated with enhancing the electric field at the surface of metal and result with enhancement around 10^{10}. Interaction between laser radiation and electrons of metal nanoparticles result with activation of SPR. The field enhancement will be greater if the plasma frequency is in resonance with the radiation. Due to the enhancement of the electric field at the surface of metal,

between two nanoparticles intense electromagnetic (EM) hot-spot begin to arise.[54] Activation of localized surface plasmon resonance with the electromagnetic field and representation of the hot spot between AuNPs is shown in Figure 1.5.

Metal nanoparticles like gold, silver and copper have SPR frequency, which is in visible and near IR range, therefore these nanoparticles are enhancing corresponding Raman scattering radiation. Effect of chemical enhancement is lower than electromagnetic enhancement theory, around 10^2. Chemical enhancement is related to molecular polarizability of the adsorbate. Figure 1.6. shows that when metal nanoparticles and analyte are combined, the highest occupied molecular orbital (HOMO) or lowest unoccupied molecular orbital (LUMO) of analyte and Fermi level of metal NPs exchange the electrons. Charge transfer interactions between analyte and metal surface results in the polarization of the molecule and Raman enhancement. Metal nanoparticles have delocalized electrons which makes them highly polarizable and compatible with SERS.[55,56,57,58]

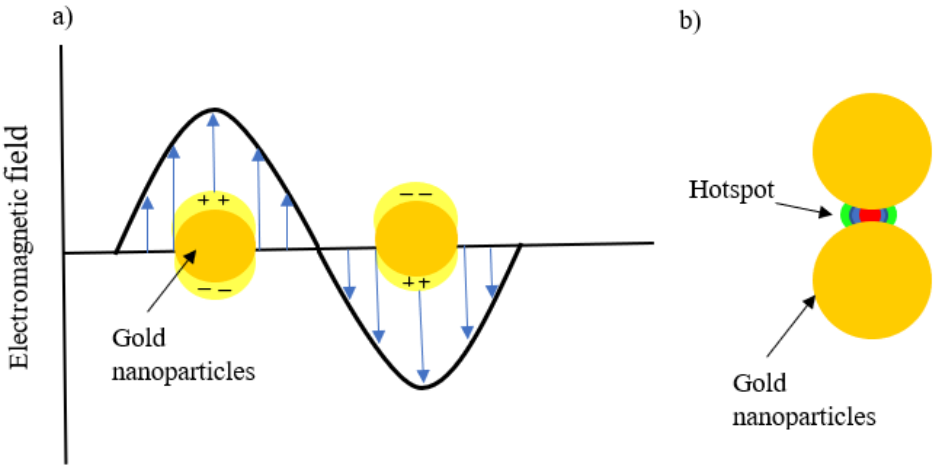

Figure 1.5. A) Activation of LSPR with electromagnetic field B) illustration of hotspot between AuNPs.[59]

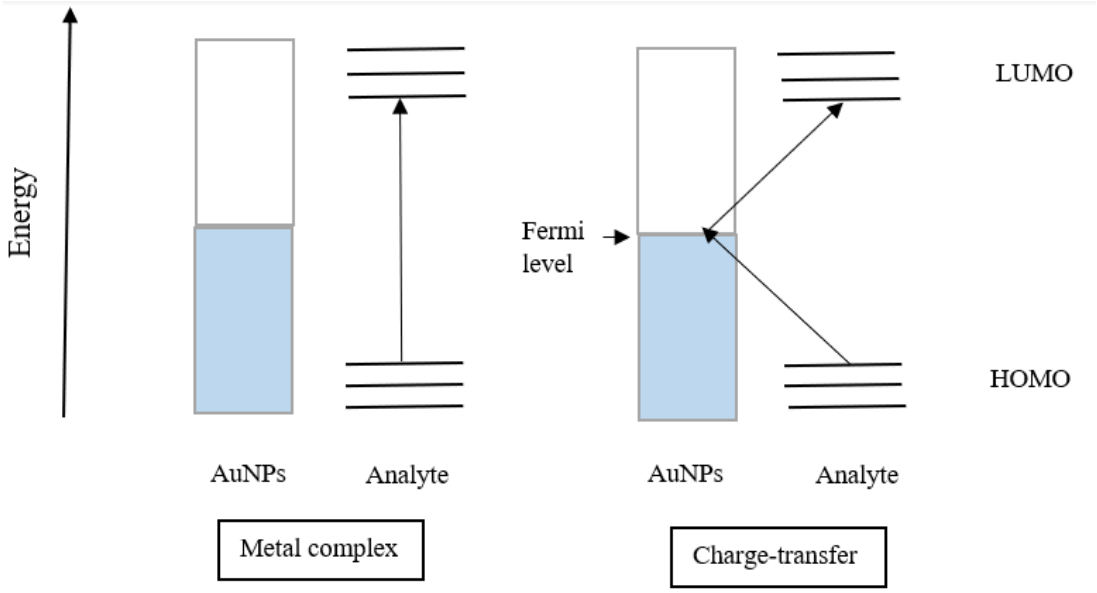

Figure 1.6. Representation of charge-transfer in chemical enhancement.[60]

There are some probe molecules that are commonly used in evaluation of SERS substrate's activity. Rhodamine 6G and crystal violet are some of the probe molecules which are used in SERS spectroscopy.[61,62] Crystal violet (CV) is known as cationic dye which is violet color. CV is used in coloring antifreeze, detergent, and textile.[63] Even though it is a Raman active molecule, peaks of CV are not detectable in low concentration with Raman spectroscopy. SERS system enable characterization of CV molecule. The chemical structure and Raman spectra of CV is given in Figure 1.7. and 1.8. respectively.

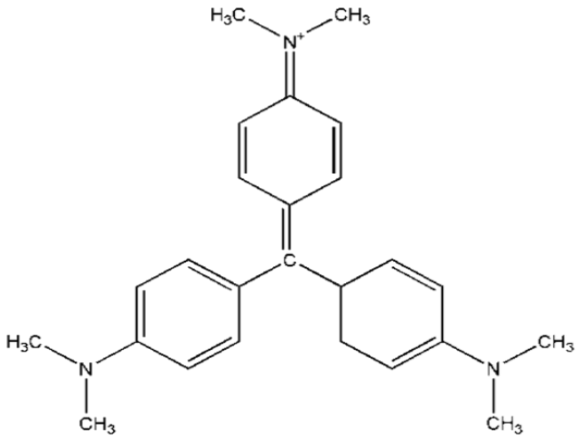

Figure 1.7. Chemical structure of crystal violet molecule

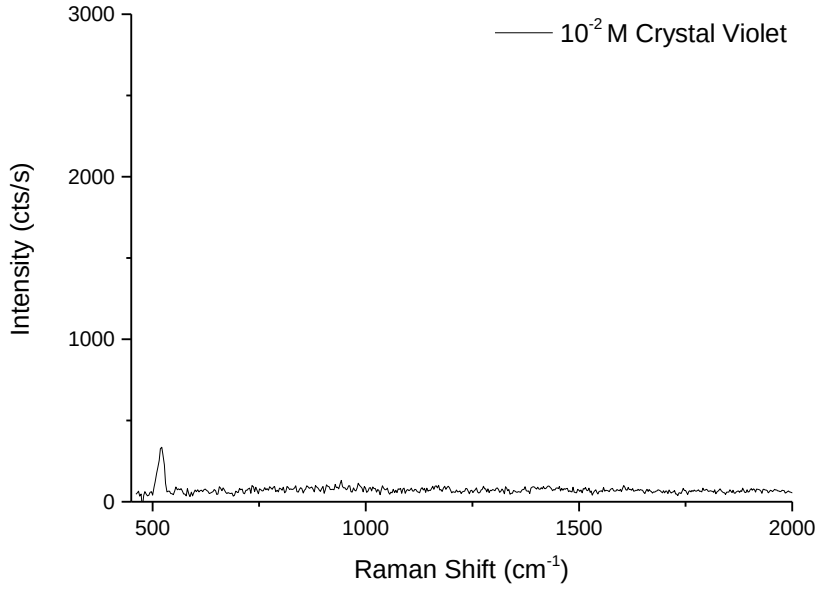

Figure 1.8. Raman spectrum of 10^{-2} M crystal violet molecule on Si-wafer. Exposure time, 0.1 s; accumulations number, 3; laser power at the sample, 20 mW, drop casting.

1.6. Quantum Dots

Quantum dots (QDs) are zero-dimensional semiconductor nanocrystals between 2 to 10 nm in length. Distinctive colors of QDs which are due to different band gaps can be tuned by size and shape. (Figure 1.9.) Their electrical and optical properties include large stokes shifts, long photostability and high brightness which gives them high potential uses in optoelectronic and electronic devices. [64,65] Core-shell structure is one of the well-known QDs due to its unique properties. Surface coating (shell) protects the core from oxidation and gives the structure stability. This increases the useful life of the particles and facilitates higher signal to noise systems achieved through increased intensity.[66]

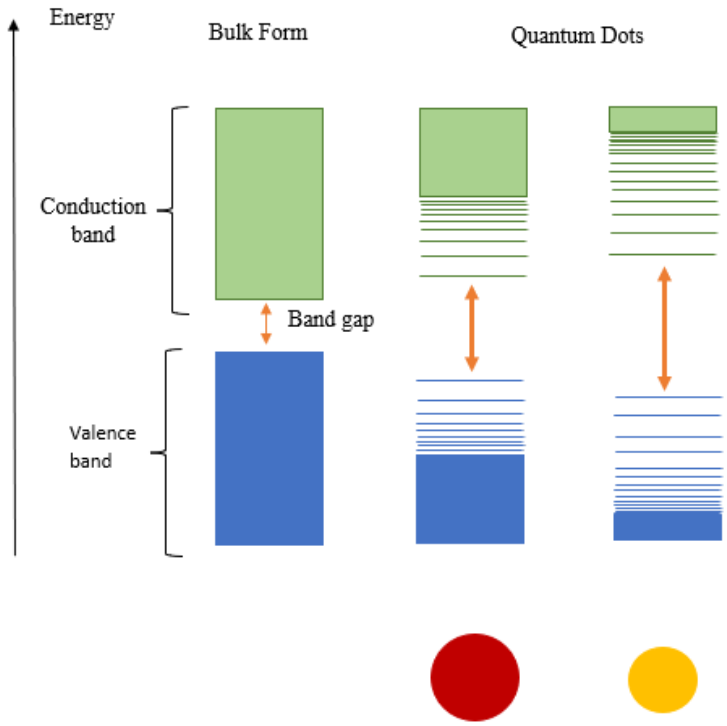

Figure 1.9. The quantum confinement effect on the energy levels in quantum dots (QDs). [67]

The utilization of semiconductor QDs in hybrid structures presents several benefits. To begin with, their absorption spectrum covers a broad range, enabling easy alignment with the spectrum of metal nanoparticle plasmons of varying sizes and materials. Conversely, the emission spectrum of QDs is narrow and distinct from their absorption spectrum. In fact, it is usually more limited than that of the plasmon, and thus, by choosing QDs of different sizes, one can adjust the exciton emission to match the plasmon resonance. Lastly, the substantial oscillator strength linked to the QD exciton facilitates the convenient execution of single object experiments.

1.8. Simulation of Hybrid Structure of AuNPs and QDs

Fano resonance is a phenomenon that arises from the interference between a broad continuum state and a narrow discrete state, manifesting as an asymmetrical, non-Lorentzian resonance. The depth of the Fano dip, which serves as a measure of the coupling strength between the localized surface plasmon resonance (LSPR) modes of nanoparticles, can be regulated through adjustments to the inter-particle gap. As the gap is increased, the coupling between the plasmon modes of each particle is diminished, leading to a gradual disappearance of the Fano dip. Conversely, in the case of a greatly reduced inter-particle gap, the coupling between the plasmon modes is significantly augmented, causing the depth of the Fano dip to approach zero, resulting in the phenomenon known as plasmon-induced transparency.[68]

When lower decay rate QDs and higher decay rate plasmonic structures are combined, Fano resonance (FR) appears as a dip in the plasmonic spectrum. FR provides control over SERS. FR allows for the extension of the lifetime of plasmon. FR also offer an extra increase in electromagnetic field localization. This has been used in signal amplification of nonlinear processes and, like a double resonance scheme, both the excited and Stokes shifted frequencies are aligned with two Fano resonances. The double FR scheme provides much stronger enhancement in the SERS signal. [69, 70,71]

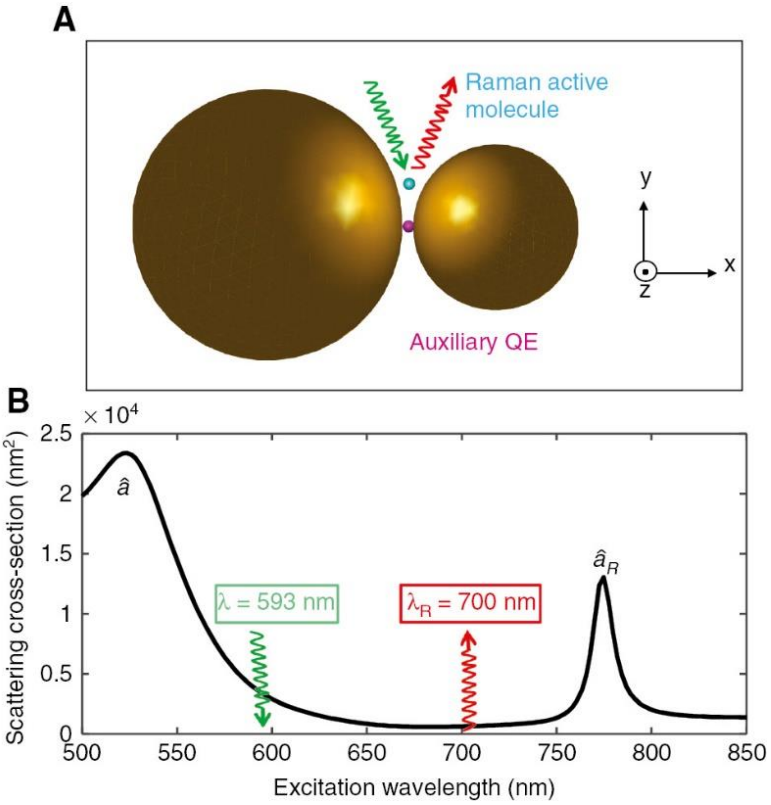

Figure 1.10. (A) The dimer system designed with double plasmon mode and Au nanoparticles (The system consists of spherical particles with 4 nm spacing and diameters of 90 nm and 55 nm, respectively). (B) Plasmonic spectrum of the Au nanoparticle dimer system. The Raman reporter molecule (blue) provides the production of the Stokes signal. The QE (purple) placed between the dimer system (hot spot) allows the Stokes signal to be increased while not changing the field strength.[12]

In the literature signal enhancement of SERS with FR relies on increasing hot spot intensity by selecting excitation and Stokes scattered wavelengths which coincide with the two Fano resonances. Selecting resonance wavelengths will be result with further enhancement of signal. This situation will extend the plasmon lifetime which

can damage the probe molecule or its vibration modes. Also, quantum tunneling effect reduces the collective oscillation of the charge carriers.[72]

The plasmon spectrum obtained for the Au dimer system proposed is shown in Figure 1.10.(B) by selecting excitation (e.g., 593 nm) and Stokes signal (e.g., 700 nm) wavelengths which does not coincide with plasmon modes. With this system, it is possible to increase the SERS signal intensity by keeping the hot-spot field strength constant. The most interesting and vital part here is neither the Raman excitation wavelength nor the QE-quantum emitter energy level range nor the evolved (Stokes) signal wavelength match the plasmon modes wavelength. Therefore, there will not be change in hot spot intensity (silent enhancement in SERS).[70]

CHAPTER 2

EXPERIMENTAL METHODOLOGY

2.1. Chemicals

Sodium tetrachloroaurate (III) dihydrate ($NaAuCl_4 \cdot 2H_2O$, >99.9%), cetyltrimethylammonium bromide (CTAB, ≥96.0%), L(+)-ascorbic acid (AA), silver nitrate ($AgNO_3$, ≥99.5%), tri-sodium citrate dihydrate ($Na_3C_6H_5O_7 \cdot 2H_2O$), hydrochloric acid (37%) were obtained from Sigma-Aldrich. Cadmium Selenide/Zinc Sulfide Quantum Dots in toluene (CdSe/ZnS, 5 mg/mL, 5 mL) was obtained from HiQ-Nano. Reactions are done under room temperature.

2.2. Characterization

Absorption spectra was obtained by Shimadzu 3600i plus model UV-Vis-NIR spectrometry which has wavelength scan range between 150-3500 nm. Fluorescence emission spectra was acquired by Cary Eclipse spectrofluorometer which has scan range between 200-1100 nm.

Characterization and morphology of Au nanostar and QD hybrid structures was obtained using the FEI NNL600I model for Focus Ion Beam (FIB) in Bilkent UNAM. The accelerating voltage in FIB systems ranges from 1 to 30 keV and the ion current is between 10 pA–30 nA. For imaging a low beam current which is between 30-50 pA was used. Energy dispersive X-ray (EDX) analysis is done by EDAX Z2e analyzer which is connected to Zeiss EVO HD15 type scanning electron microscope (SEM) in ODTÜ GÜNAM.

For SERS measurements the samples were excited through linearly polarized continuous wave (CW) 532 nm (Coherent Verdi), 660 nm and 785 nm (CNI Lasers) wavelength laser sources. Multimode (MM) fibers are coupled to a homemade microscope module including a Nikon Eclipse LV100 equipped with a 100X/0.90 NA objective. The excitation power on the sample surface is between 1 mW-20 mW. The incident polarizations of the originally linearly polarized excitation lasers are scrambled due to MM fiber delivery. The Raman signal is collected in epi-configuration by the same objective lens and coupled into another MM fiber through a beam splitter accommodating suitable dichroic mirrors (Semrock) and notch filters (Semrock). The Raman signal is analyzed by a f/9.8, 750 mm spectrometer (Andor Shamrock SR750) with 150 l/mm grating and an EMCCD camera (Andor Newton).

2.3. Synthesis of gold nanostars

2.3.1. Seed solution

Citrate-stabilized AuNPs which were obtained by Turkevich method [73] were used as seed solution. Preparation steps are followed as 0.5 mL 1% $NaAuCl_4$ was diluted to 150 mL with deionized (DI) water and solution was heated until the boiling point of solution. When boiling started, 10 mL of 1% sodium citrate solution (which is reducing agent and surfactant) was added to solution rapidly all at once. After addition of sodium citrate solution continued to boil. In an hour, solution color turned from pale yellow to ruby red, indicating the generation of stable seed AuNPs. (Figure 2.1.).

Seed solution

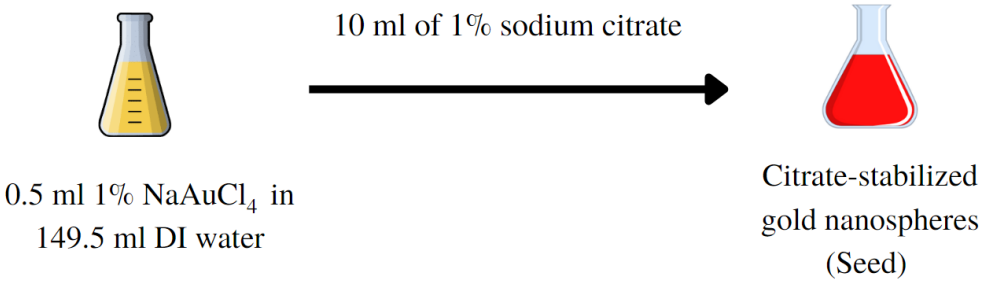

Figure 2.1. Schematic diagram of the preparation of citrate-stabilized AuNPs.

2.3.2. Growth solution

10 mL 0.001 $NaAuCl_4$ was placed in 20 mL flask and stirred constantly. 40 µL 1 M HCl and 2.5 µL Au seed which was prepared in previous step was added to the solution which was pale yellow color. 400 µL 0.003 M silver nitrate and 200 µL 0.1 M ascorbic acid were added to the mixture and color changed from pale yellow to brownish blue color. (Figure 2.2.) Addition of 2 mL 0.2 M CTAB took place at last step of procedure. The solution was mixed for another 30 minutes to complete the formation of Au nanostars. Au nanostars were separated from solution by centrifugation at 3250 rpm for 15 minutes. Supernatant was discarded and the precipitate of Au nanostars was diluted to the initial volume with DI water. This process was repeated two times.

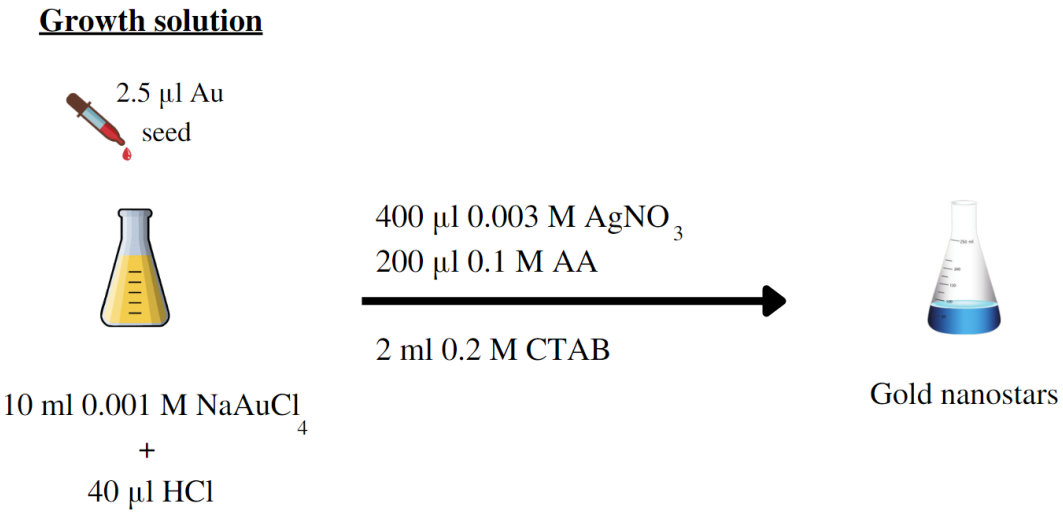

Figure 2.2. Schematic representation of synthesis of AuNPs.

2.4. Cleaning Procedure

Silicon (Si) wafers are cleaned according to a widely used three solvent procedure. Si-wafers are first washed with acetone, followed by isopropyl alcohol and finally distilled water. During each wash, the wafer is place in an ultrasonic bath for 15 minutes.

2.5. Preparation of SERS samples

2.5.1. Drop casting method

Firstly, due to high concentration of QDs, dilution is necessary, and identification of appropriate solvents and procedures. Dilution of QDs with toluene results in random drying of sample on Si-wafer and inconsistent measurements of Raman signal. The main reason of this heterogenous drying is probably the phase difference between QDs (in toluene) and Au nanostar (in deionized water).

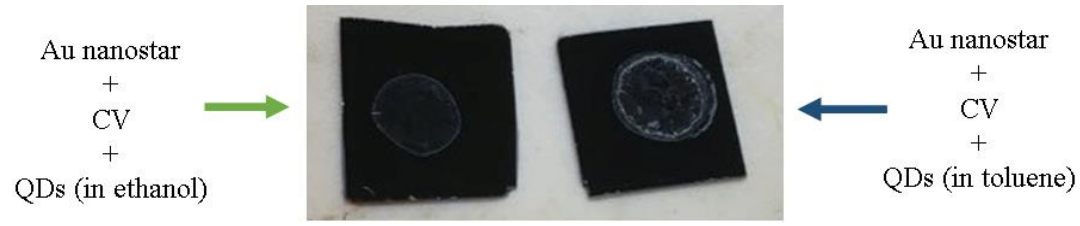

Figure 2.3. Picture of SERS samples with drop-casting method.

To remove this random drying effect QDs were diluted with ethanol. Ethanol was used as a phase transfer agent due to its polarity between toluene and deionized water. In figure 2.3 the difference between two different solvent and their drying process is shown. Due to this solvent difference all the other experiments were performed using QDs which had been diluted with ethanol to give consistent Raman signals.

5 µL of CdSe/ZnS core shell type QDs (5 mg/mL) were diluted to 1 mL solution with ethanol. The samples which contain crystal violet (CV), Au nanostars and QDs were added to Si-wafer by drop-casting method. In the first part, CV (10^{-6} M) and Au nanostars solution ($6.5x10^{10}$ particles/µL) were mixed in 1:2 (5 µL CV:10 µL Au nanostar) ratio. In the second part, QDs (0.025 mg/mL) which is diluted with ethanol were added to CV and Au nanostars solution in different volumes (1 µL, 2 µL ,3 µL ,4 µL, 5 µL etc.). 20 µL of the prepared solutions is dropped to Si-wafer surface and the samples were dried at 30℃ on hot plate. Detailed calculation for Au nanostar concentration is given in Appendix.

2.5.2. Spin coating method

To remove ring effect on the Si-wafer for samples, a spin coating method was used in order to get the solution applied to form a uniform surface on Si-wafer. Spin coated samples are prepared by multiplying the volumes of samples by 10 (100 μL Au nanostars, 50 μL CV and 20 μL, 40 μL, 60 μL QDs). The samples are accelerated for 5 s, spun for 30 s at 2000 rpm and decelerated for 3 s. This sequence of steps ensures that acceleration and deceleration are not too sudden, which would expose the sample to high sheer and could distort the resulting sample surface.

CHAPTER 3

RESULT AND DISCUSSION

3.1. Characterization of CdSe/ZnS core-shell type quantum dot decorated Au nanostars

Au nanostars are promising SERS substrates due their superior properties compared to other shapes of AuNPs. The main idea behind the SERS based on creating hot spots between nanoparticles. Anisotropic shape of Au nanostar provide strong electromagnetic field at the tips of the nanoparticles which means higher hot spot regions for the SERS substrate. Due to their outstanding properties Au nanostars are used as SERS substrates. In this study, star shaped AuNPs were synthesized by seed-mediated method.[74,75] Also, CdSe/ZnS core-shell type QDs were purchased from HiQ-Nano and used for the hybrid structure.

FIB imaging, supported by UV-Vis absorption was used to verify that AuNPs had been synthesized successfully. The EDX spectrum proves that the existence of CdSe/ZnS and Au nanostar in the final sample. Photoluminescence emission spectrum and UV-Vis absorption spectrum of CdSe/ZnS and Au nanostar hybrid structure is given to understand the interaction between these two nanostructures.

Both SEM and FIB are electron microscopy techniques that produce images of a sample by scanning the surface with a focused beam of electrons/ions. The main difference between SEM and FIB is while SEM uses a focused beam of electrons to image the sample, a FIB uses a focused beam of ions instead. For the imaging of sample FIB is preferred due to its better resolution and availability.

Figure 3.1. demonstrates FIB images of QD decorated Au Nanostars and size of Au nanostars (tip-to-tip distance) is around 67 nm. Sizes of AuNPs are between 35 nm-110 nm. The main reason of broad size distribution may be slow addition of gold seeds. To calculate the average size for AuNPs sizes of 50 different Au nanostars' size is determined by ImageJ program from FIB image and the average AuNPs (which is recorded as 67 nm) was calculated.

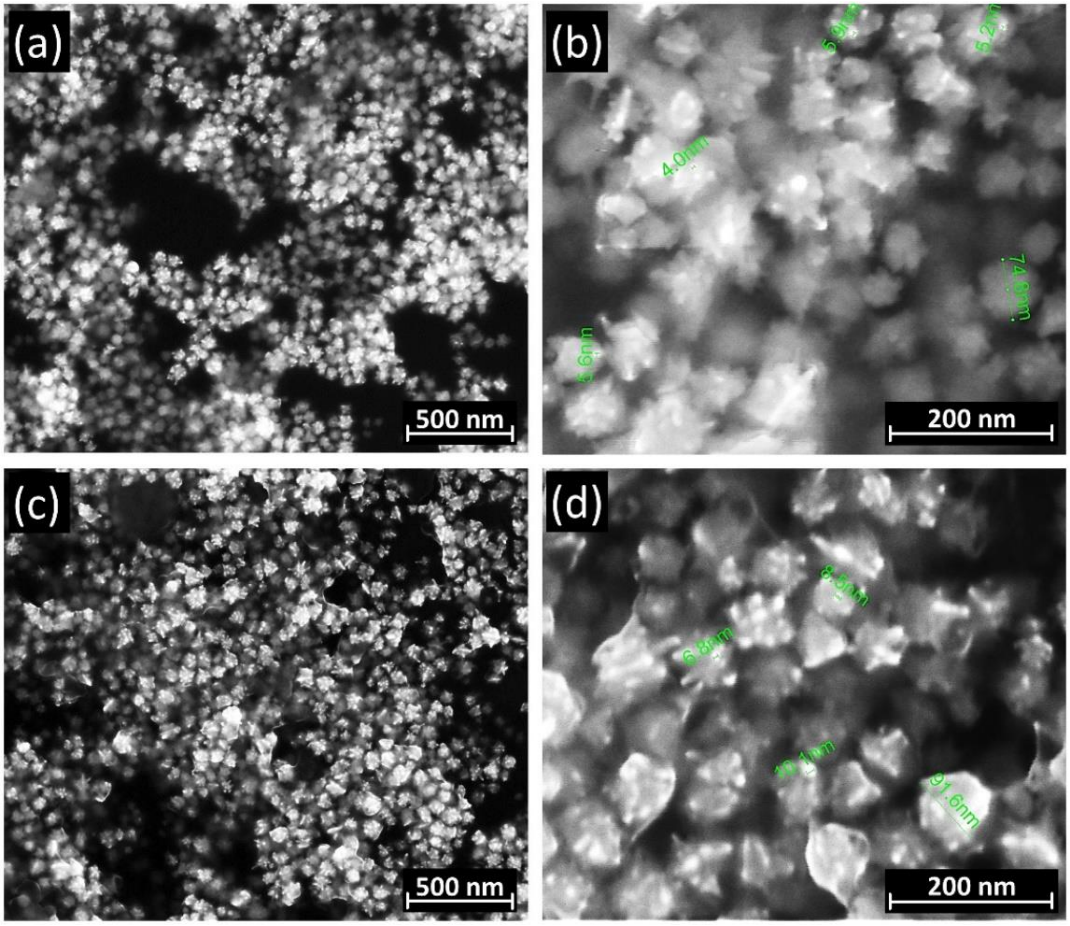

Figure 3.1.FIB images of QD decorated Au Nanostars. A) 500 nm, B) 200 nm, C)500 nm, D) 200 nm magnification with ion current 0.58 nA, accelerating voltage 15.00 kV and working distance is 5.0 mm.

The nanostars have irregular shapes with differing numbers of tips growing outside the core of nanoparticles. The bright spots on the images are characterized as QDs which are mostly located at the tips and among the nanostars. The sizes of these QDs are across a broad range from 4 to 10 nm. Finally, no additional sample preparation is performed for FIB. The samples which are prepared for SERS measurements with spin coating (on the Si wafer) are used for FIB.

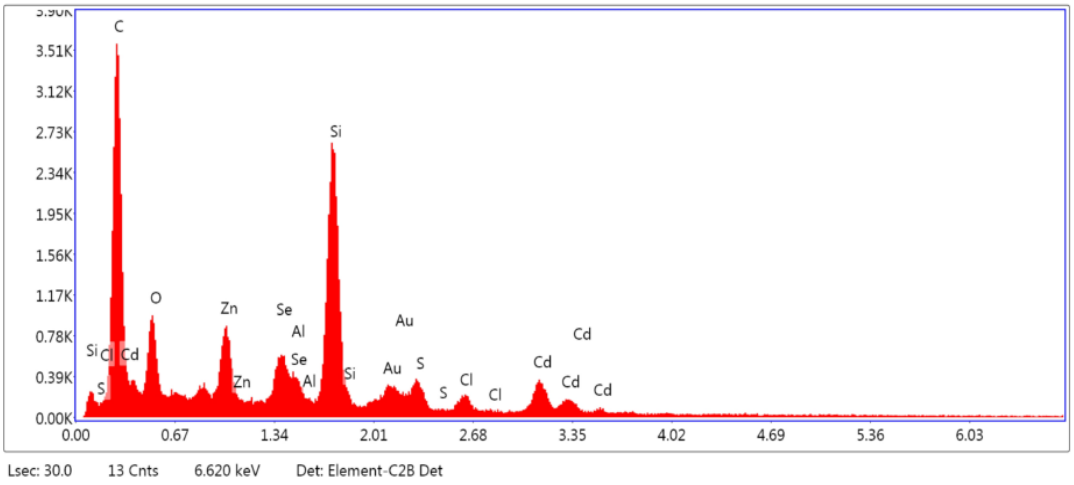

Element	Weight %	Atomic %	Net Int.	Error %	Kratio	Z	R	A	F
C K	33.98	62.61	639.02	9.91	0.1176	1.2108	0.9062	0.2858	1.0000
O K	6.61	9.14	162.21	10.45	0.0273	1.1489	0.9302	0.3590	1.0000
ZnL	7.20	2.44	136.05	5.06	0.0556	0.8258	1.0964	0.9349	0.9999
SeL	4.76	1.33	104.76	6.95	0.0345	0.7592	1.1180	0.9483	1.0068
AlK	1.93	1.59	73.06	9.26	0.0164	1.0078	0.9747	0.8383	1.0055
SiK	20.20	15.91	738.99	4.06	0.1847	1.0278	0.9819	0.8867	1.0036
AuM	6.54	0.73	80.08	10.01	0.0474	0.6076	1.2942	1.0867	1.0975
S K	3.25	2.24	83.19	7.95	0.0293	1.0026	0.9949	0.8975	1.0030
ClK	2.19	1.37	46.30	10.19	0.0193	0.9519	1.0006	0.9206	1.0043
CdL	13.34	2.63	104.84	8.47	0.0944	0.7000	1.1546	1.0039	1.0069

Figure 3.2 EDX spectrum of Au nanostars and QDs hybrid structure.

FIB analyses are supported by EDX spectrum which shows the existence of CdSe/ZnS and Au nanostars. EDX analysis provides elemental information about hybrid structure of the substrate of SERS. The data is acquired from 10 μm^2 area. Extra sample preparation was not performed for the EDX. Instead, the samples which had been dropped onto the Si-wafer surface with drop casting for SERS measurements were directly used for EDX measurements.

Existence of Al and Cl elements in the sample is most likely due to cross-contamination of the sample. The source of the Si element is the Si-wafer itself, which also acts as a wafer surface for the sample preparation step. This approach was taken, using the Si-wafer rather than a adding an alternative material, due to its distinctive Raman shift which is visualized as the sharp peak at 521 cm^{-1}. The peak of the silica does not cross with any peaks of the analyte (CV). In addition, the wafer itself has a flat and smooth surface, and it has suitable thermal conductivity that does not cause local heating when the laser hits the surface.

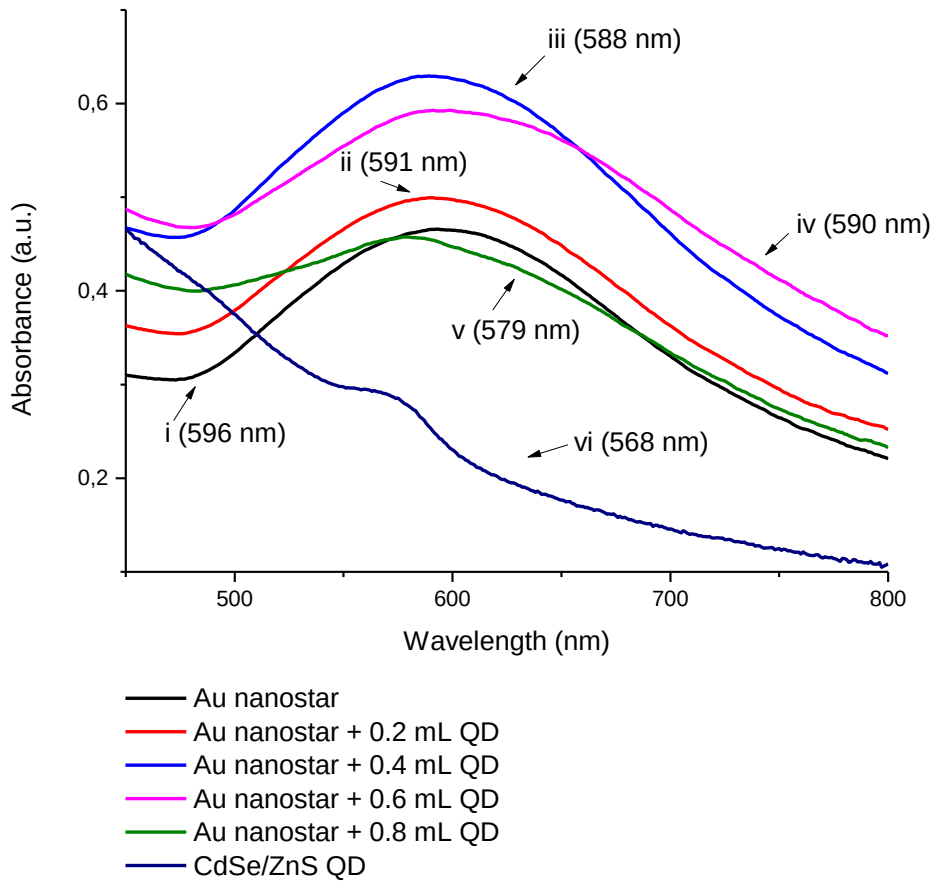

Figure 3.3. UV-Vis spectrum of Au nanostar and QDs hybrid structure prepared with the addition of different amount of QDs solution: i) 0, ii) 0.2, iii) 0.4, iv) 0.6, v) 0.8 mL and vi) 0.025 mg/mL CdSe/ZnS QD

Figure 3.3 shows UV-vis absorption spectrum of two solutions: a mixture of Au nanostars in isolation, and a mixture of QDs in combination with Au nanostars. The spectrum has broad absorption around 600 nm for both the Au nanostars and the mixture of Au nanostars combined with QDs. The breadth of this absorption band may be due to the anisotropic shape of Au nanostars. Addition of 0.2 and 0.4 mL of QDs results in a significant increase in absorption of Au nanostars due to Fano resonance (FR) between the QDs and Au nanostars. FR result in an extension of the

plasmon lifetime, which causes an increased amplitude of absorption. In addition, the half-width of the absorption curves did not change significantly, which indicates that there is no aggregation after addition of 0.2 (ii) and 0.4 mL (iii) of QDs. 0.6 mL addition (iv) of QDs does appear to cause peak broadening and a resulting decrease of absorption band intensity. This observed peak broadening and decrease in absorption may be due to aggregation of Au nanostars. Higher amounts of ethanol may decrease the surface charge of AuNPs. This decrease in zeta potential would be expected to result in the reduced agglomeration of AuNPs. Finally, the solution which contains 0.8 mL of QDs (v) has the broadest and lowest absorption compared to other solutions which have different amount QDs. Also, a distinct and visible blue shift towards absorption of QDs (vi) of the peak is observed for high amount of QDs.

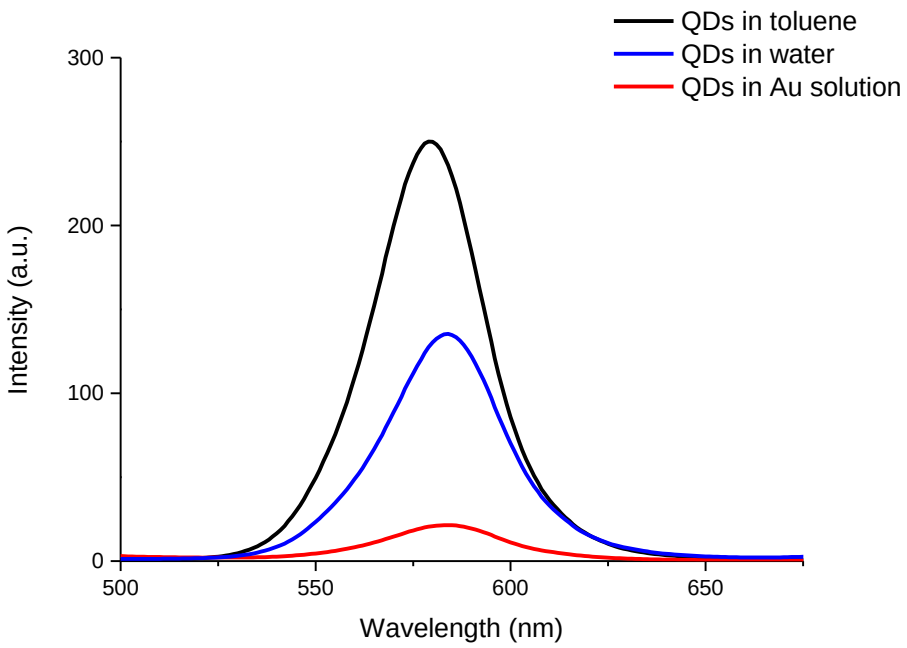

Figure 3.4. Photoluminescence emission spectrum of CdSe/ZnS in different solutions.

CdSe/ZnS type of QDs are strongly affected by nature of solvents. Interaction between polar type of solvents like alcohols and water and CdSe/ZnS result in decrease in photoluminescence (PL) intensity.[76] As it is shown in figure 3.4. PL intensity of QDs in water is lower than QDs in toluene.

QDs in Au solution have lowest intensity due to quenching. Charge transfer from QDs to Au solution result in decreasing in emission signal. [77] Figure 3.3. indicates that there is a charge transfer between QDs and Au nanostar (in water) due to intensity loss of QDs.

Compared to QDs in toluene, there is a red shift for QDs in water and QDs in Au solution. This red shift may be due to stabilization of excited state when excited state is more polar as compared to ground state, so the polar solvents stabilize excited state more than ground state. This results in reduction in the energy gap between ground and excited states, thus distinctive red shift of the band.

3.2. Surface enhanced Raman scattering properties of quantum dot decorated Au nanostars SERS studies

SERS activity of Au nanostars and QDs decorated Au nanostars were investigated using crystal violet (CV) as a probe molecule. Figure 3.4 shows SER spectra of CV adsorbed on Au nanostars and QDs decorated Au nanostars. The SER spectra show that most of the vibrational modes of CV before and after addition of QDs. The observed vibrational modes of CV molecule are in consistent with publications in the literature, allowing us to identify certain features.[78,79] The peak around 790 cm^{-1} belongs to C-H out of plane bending while ring skeletal vibrations appear between 880-1015 cm^{-1}. One of the strong peaks is between 1120-1220 cm^{-1} and it refers to C-H in plane bending. N-phenyl stretching appears around 1369 cm^{-1} and ring C-C stretching appears between 1561-1664 cm^{-1}.

In selecting a laser source, 532 nm, 660 nm and 785 nm wavelength lasers were tested as potential power sources (Figure 3.5.). A 660 nm source was ultimately selected because the peaks of crystal violet in 660 nm are more intense and therefore give a higher resolution than the other laser sources as it is shown in Figure 3.4. Low signal to noise ratio for 532 nm is due to excitation of QDs which gives background fluorescent emissions in Raman measurements, obscuring the signal peaks of crystal violet. Due to this 532 nm was not used as a power source. The 785 nm laser source was also eliminated because the energy at this wavelength is not sufficient to drive oscillation of the electrons in Au nanostars which have absorption band maximum at 676 nm. Even though there are some peaks in 785 nm they are not as intense as 660 nm therefore 660 nm laser wavelength source was identified as the most suitable for further experiments. Also, it is important to mention that the 660 nm wavelength used does not overlap with the excitation (QDs: 562 nm, Au nanostars: 577 nm) or Stokes scattered (738 nm) wavelengths of the particles. This situation supports the approach known as silent enhancement of SERS.

Background correction is not done for Figure 3.5 to show the change in background with the selected wavelength. Increase in wavelength result with decrease in background.

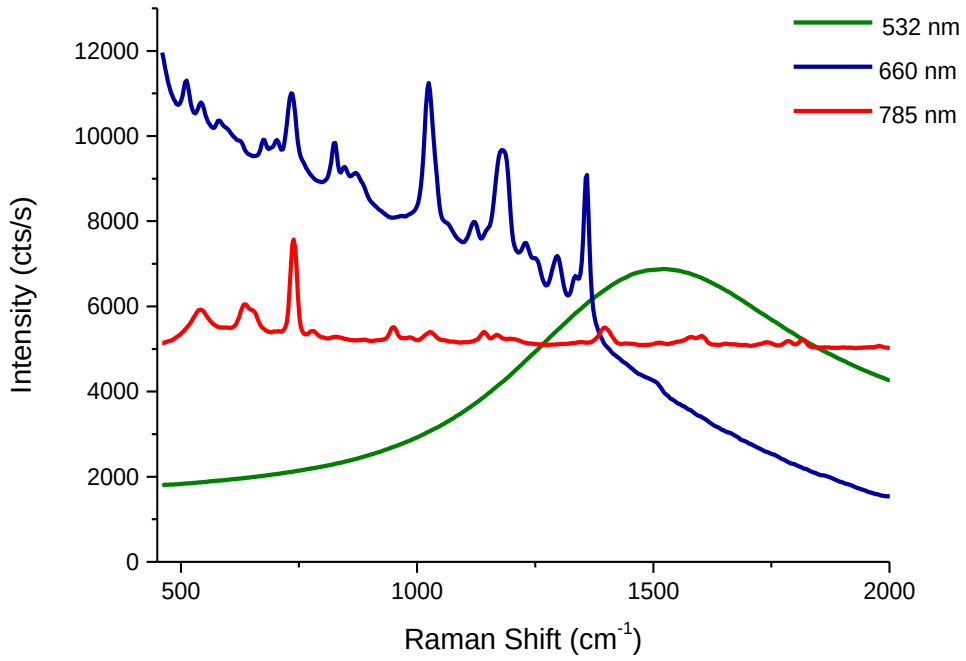

Figure 3.5. SERS spectra of 10^{-6} M CV on QD-Au nanostar collected with three different laser sources (532 nm, 660 nm and 785 nm).

After selection of laser source for further experiments, 10 measurements from the mixture were performed from different spots, to control for the ring effect in each sample resulting from the drop-casting methodology. To control for inconsistent results in measurements, the average of 10 measurements was calculated.

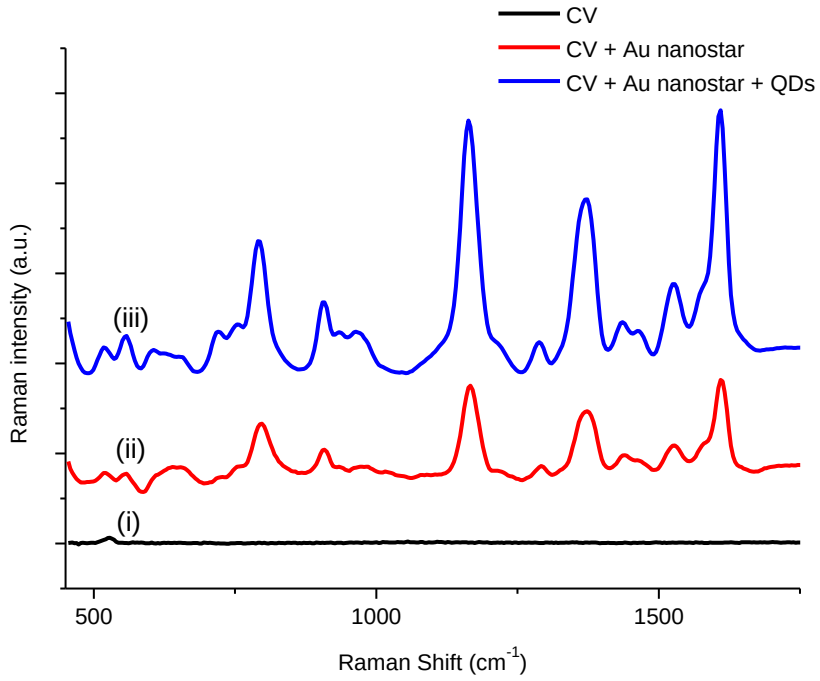

Figure 3.6. Raman spectra of 10-6 M CV (i) and SERS spectra of 10-6 M CV on (ii) Au nanostars, (iii) Au nanostars and QDs hybrid structure. Exposure time, 0.3 s; accumulations number, 3; laser power at the sample, 20 mW, drop casting.

As shown in Figure 3.6 there is a measurable enhancement of signal with addition of QDs to the Au nanostars and CV mixture. Black graph belongs to 5 µL CV (10^{-6} M), red graph is for 10 µL Au nanostar and 5 µL CV (10^{-6} M) mixture and blue one belongs to mixture of 5 µL CV (10^{-6} M), 10 µL Au nanostar and 4 µL QDs (0.025 mg/mL). To check if there is any role of QDs on enhancement of signal alone, 5 µL CV and 4 µL (0.025 mg/mL) is mixed and the measurement result is given in Figure 3.7.

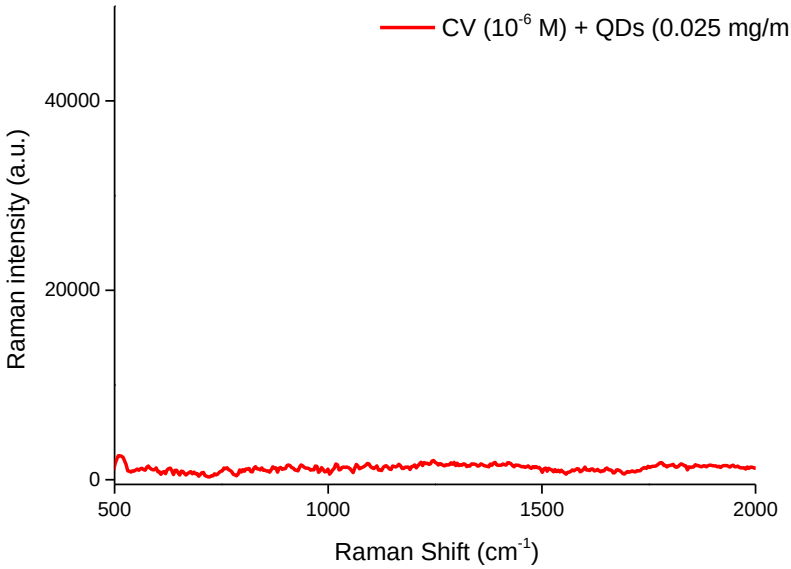

Figure 3.7. Raman spectrum of 10^{-6} M CV and 0.025 mg/mL QDs solution. Exposure time, 5 s; accumulations number, 5; laser power at the sample, 0.20 mW, drop casting.

Figure 3.7 shows that there is no significant effect of QDs in enhancement of signal for the CV molecule. Even though QDs does not contribute the signal enhancement alone, when QDs are mixed with Au nanostars the Fano resonance between these two nanostructures allows the QDs to play the role of an amplifier, contributing strongly to signal enhancement.

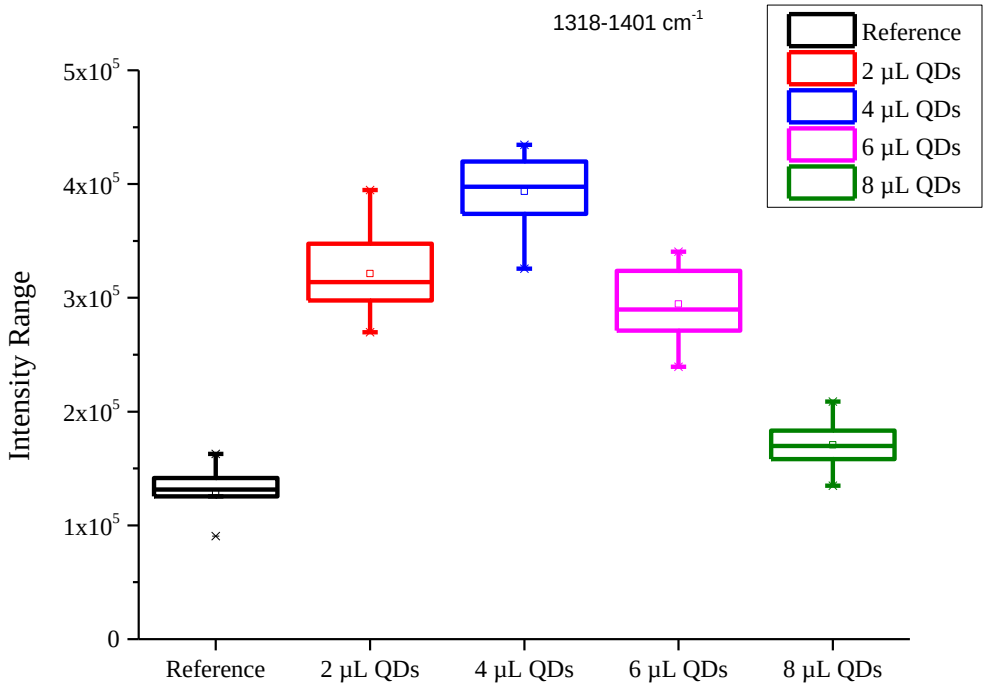

Figure 3.8. Box chart of Raman measurements for 1318-1401 cm^{-1}. Exposure time, 0.3 s; accumulations number, 3; laser power at the sample, 20 mW, drop casting.

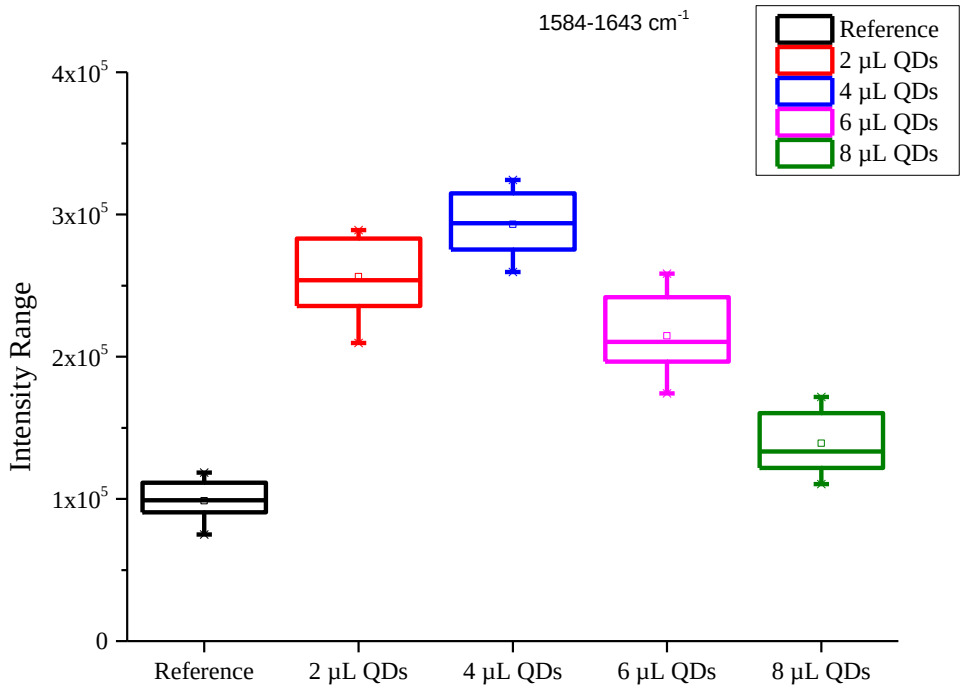

Figure 3.9. Box chart of Raman measurements for 1584-1643 cm^{-1}. Exposure time, 0.3 s; accumulations number, 3; laser power at the sample, 20 mW ,drop casting.

After collecting 10 different data points from the mixture, which is prepared with drop casting method, distribution of areas under the selected peaks are represented by the box chart in Figure 3.8. and Figure 3.9.

Figure 3.7. belongs to area under 1318-1401 cm^{-1} while Figure 3.8. is box chart of area under 1584-1643 cm^{-1}. These box charts allow us to measure signal enhancement ratio by calculation of the areas under the peaks. The mean value is given as little square in the middle of the box. The black data series belongs to CV and Au nanostar mixture which is named as reference. Reference solution contains 10 µL Au nanostar solution and 5 µL of 10^{-6} M CV. For other data series represent different amount of QDs solution addition to reference solution is shown. The red

data series show the effect of addition of 2 μL QDs to reference solution while blue, purple and green data series indicates 4 μL, 6 μL and 8 μL addition of QDs to reference solution respectively.

For 1318-1401 cm^{-1} the addition of 4 μL QDs to the mixture (5 μL CV-10 μL Au nanostar) increased the intensity range 3 times. 2 μL QDs, 6 μL and 8 μL QDs increase the intensity range 2.6, 2.2 and 1.4 respectively. Of the four different volumes tested, 4 μL of QDs addition showed the best signal enhancement for both peaks 1318-1401 cm^{-1} and 1584-1643 cm^{-1}. These two box charts shows that enhancement of different signals of CV are consistent with each other. Also, results of signal enhancement in SERS are consistent with result of UV-Vis spectrum for Au nanostar and QDs hybrid structure. In UV-Vis spectrum which is given in Figure 3.2. the highest absorption is observed when the addition of QDs is 0.4 mL which is 4 μL for SERS substance. Highest absorption of Au nanostars results with better signal enhancement while decrease in absorption and peak broadening in UV-Vis (for 0.6 and 0.8 mL) results with less enhancement compared to 0.4 mL.

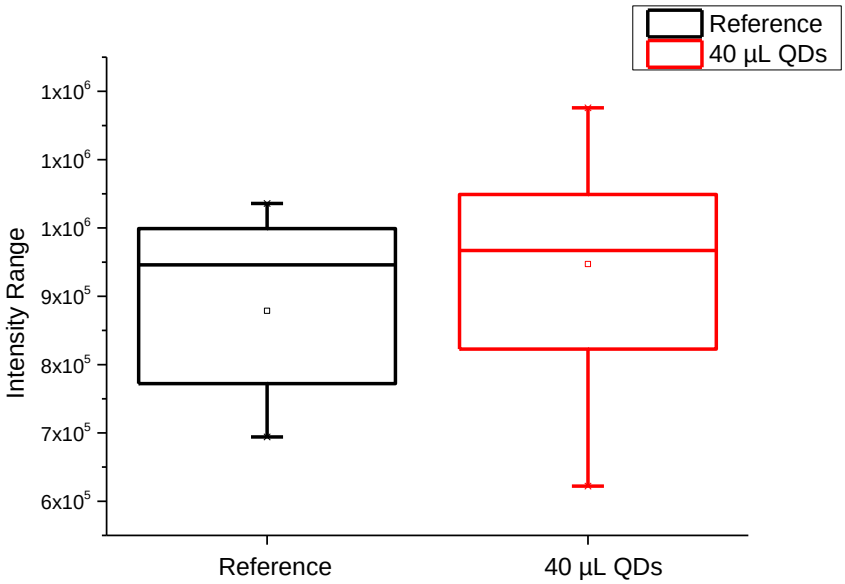

Figure 3.10. Box chart of Raman measurements for 1318-1401 cm^{-1}. Exposure time, 1 s; accumulations number, 1; laser power at the sample, 100 mW, spin coating.

After all the measurements, which are given above, were made using the drop-casting method, the measurements were repeated using spin coated samples in order to see the effect of sample homogeneity on measurements. The highest enhancement factor is provided by 4 µL addition with the drop casting method, so for measurements using the spin coating method the same conditions are used to compare both methods. Every sample amount is multiplied by 10 due to substance loss during spin coating. (100 µL Au nanostar, 50 µL CV and 40 µL QDs) Using even larger amounts of sample was one of the disadvantages of spin coating method due to the high cost and small volumes of sample which are generally used (5 mL CdSe/ZnS , HiQ Nano). In addition, Figure 3.9 shows clearly that the distribution area is between 1318-1401 cm^{-1} peak. Compared to drop casting method spin coating clearly results in a wider distribution. For the reference in Figure 3.10 while highest area is around $1x10^6$ the lowest area is $7 x10^5$. There is $3x10^5$ difference between the highest and lowest area under the peak between 1318-1401 cm^{-1}. Figure 3.7 shows

that the distribution difference is $5x10^4$ which is almost 6 times lower than spin coated version.

One reason for the observed low enhancement and wide distribution may be the agglomeration of particles during the spin process due to mass difference between QDs and Au nanostars. This shows that using the drop casting method for measurements will give more reliable results. The majority of the measurements are done using the drop casting method instead of spin coating method due to this disadvantage of spin coating.

The final results validated a clear protocol for the generation and excitation of Au nanostars/QDs hybrid structure. The results of this project clearly demonstrated the signal amplification (of approximately 3 times more with existing techniques) possible using a 660 nm laser source and combination of 4 μL of QDs (0.025 mg/mL) to 10 μL of Au nanostar solution (drop casting method). The hybrid structure was also tested with different types of star nanoparticles which have different absorption properties. Finally, the calculated enhancement factor (EF) for Au nanostar and CV solution is calculated as $1.83x10^7$. Details of EF calculation and other SERS measurements with different Au nanostars are given in Appendix.

CHAPTER 4

CONCLUSION

Gold nanoparticles have numerous application areas due to their unique properties. Sensing, imaging. solar cells and drug delivery are some of the application areas of AuNPs. Au nanostar are one of the well-known shapes of AuNPs due to their broad absorption in visible region and anisotropic shapes.

Quantum dots are type of semiconductor nanocrystals and they are in a limelight due to their promising optical properties. These properties give them potential application fields like bioimaging, solar cells and biosensing.

In literature hybrid structures of both Au nanostar and QDs are investigated separately however not much research has been done on combining both QDs and Au nanostar to be used as a SERS substrate.

In this study, SERS of crystal violet with Au nanostars and quantum dot hybrid structures has been investigated. The hybrid structure was successfully characterized by UV-Vis, PL spectroscopy and FIB. FIB imaging reveals the formation of Au nanostar and existence of QDs in mixture. UV-Vis and PL spectrum help to understand the interaction between Au nanostar and QDs hybrid structure.

The intensity range is around $1.3x10^5$ when using Au nanostar as a SERS substrate. The addition of QDs to the mixture increases the intensity to $3.9x10^5$ which is roughly 3 times larger than Au nanostars alone. SERS signal is increased a further 3 times with the use of the hybrid structure.

For the future work shorter surfactant can be used in synthesis of Au nanostars to decrease the size between Au nanostar and QDs. Decreasing size difference between these two nanostructures may increase the interaction between them. The same

protocols can be applied to QDs in aqueous phase and Au nanostar to remove the phase difference in the drying process. Furthermore, QDs and Au nanostars can be decorated by amide and carboxylic acid to connect them with amide bond to each other. This may increase the interaction and hot spot intensity between them.

These results reveal a promising direction for future work and validate the core concept that QD/Au nanostar hybrid structures can be used to significantly improve the SERS signal to noise ratio of AuNPs, which has been a critical barrier to wider application of AuNPs industrially.

REFERENCES

[1] Khan, A. K., Rashid, R., Murtaza, G., & Zahra, A. (2014). Gold nanoparticles: Synthesis and applications in drug delivery. *Tropical Journal of Pharmaceutical Research*, *13*(7), 1169. https://doi.org/10.4314/tjpr.v13i7.23

[2] Wang, K., Li, S., Petersen, M., Wang, S., & Lu, X. (2018). Detection and characterization of antibiotic-resistant bacteria using surface-enhanced Raman spectroscopy. *Nanomaterials*, *8*(10), 762. https://doi.org/10.3390/nano8100762

[3] Mohan, S., sekar, A. C., & Subramanian, B. (2014). Surface Enhanced Raman scattering studies of silver-Gold Normal and inverted core-shell nanostructures on their efficiency of detecting molecules. *Procedia Engineering*, *92*, 19–25. https://doi.org/10.1016/j.proeng.2013.10.005

[4] Zhang, L., Guan, C., Wang, Y., & Liao, J. (2016). Highly effective and uniform sers substrates fabricated by etching multi-layered gold nanoparticle arrays. *Nanoscale*, *8*(11), 5928–5937. https://doi.org/10.1039/c6nr00502k

[5] Li, H., Liu, H., Qin, Y., Mu, Y., Fang, X., Zhai, T., & Zhang, X. (2020). Gold-stabilized gold–silver alloy nanostructures as high-performance SERS substrate. *Plasmonics*, *15*(6), 2027–2032. https://doi.org/10.1007/s11468-020-01229-0

[6] Hacıefendioğlu, T., Balıkoğlu, B., Aydın, F., Kolay, İ., Öztürk, İ. M., & Asil, D. (2021). Enhanced photocurrent in pbse nanorod-quantum dot bulk nano-heterojunction solar cells. *Journal of Materials Science: Materials in Electronics*, *33*(2), 714–724. https://doi.org/10.1007/s10854-021-07342-y

[7] Mews, A., & Zhao, J. (2007). A bright outlook for Quantum Dots. *Nature Photonics*, *1*(12), 683–684. https://doi.org/10.1038/nphoton.2007.239

[8] Sablon, K. A., Little, J. W., Mitin, V., Sergeev, A., Vagidov, N., & Reinhardt, K. (2011). Strong enhancement of solar cell efficiency due to quantum dots with built-in charge. *Nano Letters*, *11*(6), 2311–2317. https://doi.org/10.1021/nl200543v

[9] Kauranen, M., & Zayats, A. V. (2012). Nonlinear plasmonics. *Nature Photonics*, *6*(11), 737–748. https://doi.org/10.1038/nphoton.2012.244

[10] Zhong, J.-H., Vogelsang, J., Yi, J.-M., Wang, D., Wittenbecher, L., Mikaelsson, S., Korte, A., Chimeh, A., Arnold, C. L., Schaaf, P., Runge, E., Huillier, A. L., Mikkelsen, A., & Lienau, C. (2020). Nonlinear plasmon-exciton coupling enhances sum-frequency generation from a hybrid metal/semiconductor nanostructure. *Nature Communications*, *11*(1). https://doi.org/10.1038/s41467-020-15232-w

[11] Dutta, A., Alam, K., Nuutinen, T., Hulkko, E., Karvinen, P., Kuittinen, M., Toppari, J. J., & Vartiainen, E. M. (2019). Influence of fano resonance on SERS enhancement in Fano-plasmonic oligomers. *Optics Express*, *27*(21), 30031. https://doi.org/10.1364/oe.27.030031

[12] Ye, J., Wen, F., Sobhani, H., Lassiter, J. B., Van Dorpe, P., Nordlander, P., & Halas, N. J. (2012). Plasmonic nanoclusters: Near field properties of the Fano resonance interrogated with Sers. *Nano Letters*, *12*(3), 1660–1667. https://doi.org/10.1021/nl3000453

[13] Zhu, W., & Crozier, K. B. (2014). Quantum mechanical limit to plasmonic enhancement as observed by surface-enhanced Raman scattering. *Nature Communications*, *5*(1). https://doi.org/10.1038/ncomms6228

[14] Song, Y., Huang, H.-C., Lu, W., Li, N., Su, J., Cheng, S.-B., Lai, Y., Chen, J., & Zhan, J. (2021). Ag@WS2 quantum dots for surface enhanced Raman spectroscopy: Enhanced charge transfer induced highly sensitive detection of thiram from honey and beverages. *Food Chemistry*, *344*, 128570. https://doi.org/10.1016/j.foodchem.2020.128570

[15] Pinkhasova, P., Yang, L., Zhang, Y., Sukhishvili, S., & Du, H. (2012). Differential SERS activity of gold and silver nanostructures enabled by adsorbed poly(vinylpyrrolidone). *Langmuir*, *28*(5), 2529–2535. https://doi.org/10.1021/la2047992

[16] Franciscato, D. S., Matias, T. A., Shinohara, J., Gonçalves, J. M., Coelho, N. P., Fernandes, C. S., Basso, E. A., Nakatani, H. S., Araki, K., Toma, H. E., & de Souza, V. R. (2018). Thiosemicarbazone@Gold nanoparticle hybrid as selective SERS substrate for HG2+ ions. *Spectrochimica Acta Part A: Molecular and Biomolecular Spectroscopy*, *204*, 174–179. https://doi.org/10.1016/j.saa.2018.06.038

[17] Elci, A., Demirtas, O., Ozturk, I. M., Bek, A., & Nalbant Esenturk, E. (2018). Synthesis of tin oxide-coated gold nanostars and evaluation of their surface-enhanced Raman scattering activities. *Journal of Materials Science*, *53*(24), 16345–16356. https://doi.org/10.1007/s10853-018-2792-4

[18] Du, Y., Zhao, Y., Qu, Y., Chen, C.-H., Chen, C.-M., Chuang, C.-H., & Zhu, Y. (2014). Enhanced light–matter interaction of graphene–gold nanoparticle hybrid films for high-performance SERS detection. *J. Mater. Chem. C*, *2*(23), 4683–4691. https://doi.org/10.1039/c4tc00353e

[19] Fang, P.-P., Li, J.-F., Yang, Z.-L., Li, L.-M., Ren, B., & Tian, Z.-Q. (2008). Optimization of SERS activities of gold nanoparticles and gold-core-palladium-shell nanoparticles by controlling size and shell thickness. *Journal of Raman Spectroscopy*, *39*(11), 1679–1687. https://doi.org/10.1002/jrs.2066

[20] Tao, Z. (2013, September 17). *Plasmon exciton interaction in gold nanostructure and quantum dot conjugate and its applications in Biosensing*. NUS. Retrieved August 16, 2022, from http://scholarbank.nus.edu.sg/handle/10635/118896

[21] Tian, F., Bonnier, F., Casey, A., Shanahan, A. E., & Byrne, H. J. (2014). Surface enhanced Raman scattering with gold nanoparticles: Effect of particle shape. *Anal. Methods*, *6*(22), 9116–9123. https://doi.org/10.1039/c4ay02112f

[22] Lai, C.-H., Wang, G.-A., Ling, T.-K., Wang, T.-J., Chiu, P.-kai, Chou Chau, Y.-F., Huang, C.-C., & Chiang, H.-P. (2017). Near infrared surface-enhanced Raman scattering based on star-shaped gold/silver nanoparticles and hyperbolic metamaterial. *Scientific Reports*, *7*(1). https://doi.org/10.1038/s41598-017-05939-0

[23] Kozanoglu, D., Apaydin, D. H., Cirpan, A., & Nalbant, E. (2013). Power conversion efficiency enhancement of organic solar cells by addition of gold nanostars, nanorods, and Nanospheres. *Organic Electronics*, *14*(7), 1720–1727. https://doi.org/10.1016/j.orgel.2013.04.008

[24] Horikoshi, S.; Serpone, N. Introduction to Nanoparticles. In Microwaves in Nanoparticle Synthesis; Wiley-VCH Verlag GmbH & Co. KGaA: Weinheim, Germany, 2013; pp 1–24.

[25] Corma, A., & Garcia, H. (2008). Supported gold nanoparticles as catalysts for organic reactions. *Chemical Society Reviews*, *37*(9), 2096. https://doi.org/10.1039/b707314n

[26] Lin, W. (2015). Introduction: Nanoparticles in medicine. *Chemical Reviews*, *115*(19), 10407–10409. https://doi.org/10.1021/acs.chemrev.5b00534

[27] Zhang, X. (2015). Gold nanoparticles: Recent advances in the biomedical applications. *Cell Biochemistry and Biophysics*, *72*(3), 771–775. https://doi.org/10.1007/s12013-015-0529-4

[28] Das, M., Shim, K. H., An, S. S., & Yi, D. K. (2011). Review on gold nanoparticles and their applications. *Toxicology and Environmental Health Sciences*, *3*(4), 193–205. https://doi.org/10.1007/s13530-011-0109-y

[29] Petryayeva, E., & Krull, U. J. (2011). Localized surface plasmon resonance: Nanostructures, bioassays and Biosensing—a review. *Analytica Chimica Acta*, *706*(1), 8–24. https://doi.org/10.1016/j.aca.2011.08.020

[30] Ou, J., Zhou, Z., Chen, Z., & Tan, H. (2019). Optical diagnostic based on functionalized gold nanoparticles. *International Journal of Molecular Sciences*, *20*(18), 4346. https://doi.org/10.3390/ijms20184346

[31] Panikkanvalappil, R. S.; Theruvakkattil, S. S.; Samal, A. K.; Thalappil, P. ChemInform Abstract: Anisotropic Nanomaterials: Structure, Growth, Assembly, and Functions. ChemInform 2011, 42 (24), no-no.

[32] Pal Singh, J.; Kumar, M.; Sharma, A.; Pandey, G.; Chae, K. H.; Lee, S. Bottom-up and Top-down Approaches for MgO. In *Sonochemical Reactions*; IntechOpen, 2020.

[33] *Complex-Shaped Metal Nanoparticles: Bottom-up Syntheses and Applications*, 1st ed.; Sau, T. K., Rogach, A. L., Eds.; Wiley-VCH Verlag: Weinheim, Germany, 2012.

[34] Reetz, M. T.; Helbig, W. Size-Selective Synthesis of Nanostructured Transition Metal Clusters. *J. Am. Chem. Soc.* **1994**, *116* (16), 7401–7402.

[35] Huang, C.-J.; Chiu, P.-H.; Wang, Y.-H.; Chen, K.-L.; Linn, J.-J.; Yang, C.-F. Electrochemically Controlling the Size of Gold Nanoparticles. *J. Electrochem. Soc.* **2006**, *153* (12), D193.

[36] Shah, M. Gold Nanoparticles: Various Methods of Synthesis and Antibacterial Applications. *Front. Biosci.* **2014**, *19* (8), 1320.

[37] Herizchi, R.; Abbasi, E.; Milani, M.; Akbarzadeh, A. Current Methods for Synthesis of Gold Nanoparticles. *Artif. Cells Nanomed. Biotechnol.* **2016**, *44* (2), 596–602.

[39] Frens, G. Controlled Nucleation for the Regulation of the Particle Size in Monodisperse Gold Suspensions. *Nat. Phys. Sci.* **1973**, *241* (105), 20–22.

[40] Zhao, P.; Li, N.; Astruc, D. State of the Art in Gold Nanoparticle Synthesis. *Coord. Chem. Rev.* **2013**, *257* (3–4), 638–665.

[41] Slepička, P.; Slepičková Kasálková, N.; Siegel, J.; Kolská, Z.; Švorčík, V. Methods of Gold and Silver Nanoparticles Preparation. *Materials (Basel)* **2019**, *13* (1), 1.

[42] Brust, M.; Walker, M.; Bethell, D.; Schiffrin, D. J.; Whyman, R. Synthesis of Thiol-Derivatised Gold Nanoparticles in a Two-Phase Liquid–Liquid System. *J. Chem. Soc. Chem. Commun.* **1994**, *0* (7), 801–802.

[43] Elimelech, M.; Gregory, J.; Jia, X.; Williams, R. A. Surface Interaction Potentials. In Particle Deposition & Aggregation; Elsevier, 1995; pp 33–67.

[44] Hierrezuelo, J.; Sadeghpour, A.; Szilagyi, I.; Vaccaro, A.; Borkovec, M. Electrostatic Stabilization of Charged Colloidal Particles with Adsorbed Polyelectrolytes of Opposite Charge. *Langmuir* **2010**, *26* (19), 15109–15111.

[45] Navlani-García, M.; Salinas-Torres, D.; Mori, K.; Kuwahara, Y.; Yamashita, H. Tailoring the Size and Shape of Colloidal Noble Metal Nanocrystals as a Valuable Tool in Catalysis. Catal. Surv. Asia 2019, 23 (3), 127–148.

[46] Smith, D. K.; Korgel, B. A. The Importance of the CTAB Surfactant on the Colloidal Seed-Mediated Synthesis of Gold Nanorods. *Langmuir* **2008**, *24* (3), 644–649.

[47] Gole, A.; Murphy, C. J. Seed-Mediated Synthesis of Gold Nanorods: Role of the Size and Nature of the Seed. *Chem. Mater.* **2004**, *16* (19), 3633–3640.

[48] Gala, U.; Chauhan, H. Principles and Applications of Raman Spectroscopy in Pharmaceutical Drug Discovery and Development. *Expert Opin. Drug Discov.* **2015**, *10* (2), 187–206.

[49] Moura, C. C.; Tare, R. S.; Oreffo, R. O. C.; Mahajan, S. Raman Spectroscopy and Coherent Anti-Stokes Raman Scattering Imaging: Prospective Tools for Monitoring Skeletal Cells and Skeletal Regeneration. *J. R. Soc. Interface* **2016**, *13* (118). https://doi.org/10.1098/rsif.2016.0182.

[50] Lupoi, J. S., Gjersing, E., & Davis, M. F. (2015). Evaluating lignocellulosic biomass, its derivatives, and downstream products with Raman spectroscopy. *Frontiers in Bioengineering and Biotechnology*, *3*. https://doi.org/10.3389/fbioe.2015.00050

[51] Vankeirsbilck, T.; Vercauteren, A.; Baeyens, W.; Van der Weken, G.; Verpoort, F.; Vergote, G.; Remon, J. P. Applications of Raman Spectroscopy in Pharmaceutical Analysis. *Trends Analyt. Chem.* **2002**, *21* (12), 869–877.

[52] Valpapuram, I.; Candeloro, P.; Coluccio, M. L.; Parrotta, E. I.; Giugni, A.; Das, G.; Cuda, G.; Di Fabrizio, E.; Perozziello, G. Waveguiding and SERS Simplified Raman Spectroscopy on Biological Samples. *Biosensors (Basel)* **2019**, *9* (1), 37.

[53] Pérez-Jiménez, A. I.; Lyu, D.; Lu, Z.; Liu, G.; Ren, B. Surface-Enhanced Raman Spectroscopy: Benefits, Trade-Offs and Future Developments. *Chem. Sci.* **2020**, *11* (18), 4563–4577.

[54] Kumar, S.; Kumar, P.; Das, A.; Shakher Pathak, C. Surface-Enhanced Raman Scattering: Introduction and Applications. In *Recent Advances in Nanophotonics - Fundamentals and Applications*; IntechOpen, 2020.

[55] *Nanoplasmonics - Fundamentals and Applications*; Barbillon, G., Ed.; InTech, 2017.

[56] Sitjar, J.; Liao, J.-D.; Lee, H.; Liu, B. H.; Fu, W.-E. SERS-Active Substrate with Collective Amplification Design for Trace Analysis of Pesticides. *Nanomaterials (Basel)* **2019**, *9* (5). https://doi.org/10.3390/nano9050664.

[57] Langer, J.; Jimenez de Aberasturi, D.; Aizpurua, J.; Alvarez-Puebla, R. A.; Auguié, B.; Baumberg, J. J.; Bazan, G. C.; Bell, S. E. J.; Boisen, A.; Brolo, A. G.; Choo, J.; Cialla-May, D.; Deckert, V.; Fabris, L.; Faulds, K.; García de Abajo, F. J.; Goodacre, R.; Graham, D.; Haes, A. J.; Haynes, C. L.; Huck, C.; Itoh, T.; Käll, M.; Kneipp, J.; Kotov, N. A.; Kuang, H.; Le Ru, E. C.; Lee, H. K.; Li, J.-F.; Ling, X. Y.; Maier, S. A.; Mayerhöfer, T.; Moskovits, M.; Murakoshi, K.; Nam, J.-M.; Nie, S.; Ozaki, Y.; Pastoriza-Santos, I.; Perez-Juste, J.; Popp, J.; Pucci, A.; Reich, S.; Ren, B.; Schatz, G. C.; Shegai, T.; Schlücker, S.; Tay, L.-L.; Thomas, K. G.; Tian, Z.-Q.; Van Duyne, R. P.; Vo-Dinh, T.; Wang, Y.; Willets, K. A.; Xu, C.; Xu, H.; Xu, Y.; Yamamoto, Y. S.; Zhao, B.; Liz-Marzán, L. M. Present and Future of Surface-Enhanced Raman Scattering. *ACS Nano* **2020**, *14* (1), 28–117. https://doi.org/10.1021/acsnano.9b04224.

[58] Campanella, B.; Palleschi, V.; Legnaioli, S. Introduction to Vibrational Spectroscopies. *ChemTexts* **2021**, *7* (1). https://doi.org/10.1007/s40828-020-00129-4.

[59] Zong, C., Xu, M., Xu, L.-J., Wei, T., Ma, X., Zheng, X.-S., Hu, R., & Ren, B. (2018). Surface-enhanced Raman spectroscopy for bioanalysis: Reliability and challenges. *Chemical Reviews*, *118*(10), 4946–4980. https://doi.org/10.1021/acs.chemrev.7b00668

[60] Chu, H., Song, S., Li, C., & Gibson, D. (2017). Surface enhanced Raman scattering substrates made by oblique angle deposition: Methods and applications. *Coatings*, *7*(2), 26. https://doi.org/10.3390/coatings7020026

[61] Kahraman, M., Daggumati, P., Kurtulus, O., Seker, E., & Wachsmann-Hogiu, S. (2013). Fabrication and characterization of flexible and tunable plasmonic nanostructures. *Scientific Reports*, *3*(1). https://doi.org/10.1038/srep03396

[62] Kneipp, J., Kneipp, H., Wittig, B., & Kneipp, K. (2010). Novel optical nanosensors for probing and imaging live cells. *Nanomedicine: Nanotechnology, Biology and Medicine*, *6*(2), 214–226. https://doi.org/10.1016/j.nano.2009.07.009

[63] Fateixa, S., Nogueira, H. I., & Trindade, T. (2018). Surface-enhanced Raman scattering spectral imaging for the attomolar range detection of crystal violet in contaminated water. *ACS Omega*, *3*(4), 4331–4341. https://doi.org/10.1021/acsomega.7b01983

[64] Chung, E. J., Leon, L., & Rinaldi, C. (Eds.). (2019). *Nanoparticles for biomedical applications: Fundamental concepts, biological interactions and clinical applications*. Elsevier Science Publishing.

[65] McKittrick, J., & Shea-Rohwer, L. E. (2014). Review: Down conversion materials for solid-state lighting. *Journal of the American Ceramic Society. American Ceramic Society*, *97*(5), 1327–1352. https://doi.org/10.1111/jace.12943

[66] Hao, J.-jie, Zhou, J., & Zhang, C.-yang. (2013). A tri-n-octylphosphine-assisted successive ionic layer adsorption and reaction method to synthesize multilayered core–shell cdse–zns quantum dots with extremely high quantum yield. *Chemical Communications*, *49*(56), 6346. https://doi.org/10.1039/c3cc43147a

[67] Brkić, S. (2018). Applicability of quantum dots in biomedical science. *Ionizing Radiation Effects and Applications*. https://doi.org/10.5772/intechopen.71428

[68] Dutta, A., Alam, K., Nuutinen, T., Hulkko, E., Karvinen, P., Kuittinen, M., Toppari, J. J., & Vartiainen, E. M. (2019). Influence of fano resonance on SERS enhancement in Fano-plasmonic oligomers. *Optics Express*, *27*(21), 30031. https://doi.org/10.1364/oe.27.030031

[69] Ye, J., Wen, F., Sobhani, H., Lassiter, J. B., Van Dorpe, P., Nordlander, P., & Halas, N. J. (2012). Plasmonic nanoclusters: Near field properties of the Fano

resonance interrogated with Sers. *Nano Letters*, *12*(3), 1660–1667. https://doi.org/10.1021/nl3000453

[70] Postaci, S., Yildiz, B. C., Bek, A., & Tasgin, M. E. (2018). Silent enhancement of SERS signal without increasing hot spot intensities. *Nanophotonics*, *7*(10), 1687–1695. https://doi.org/10.1515/nanoph-2018-0089

[71] Turkpence, D., Akguc, G. B., Bek, A., & Tasgin, M. E. (2014). Engineering nonlinear response of nanomaterials using Fano resonances. *Journal of Optics*, *16*(10), 105009. https://doi.org/10.1088/2040-8978/16/10/105009

[72] Ma, W., Dai, Q., Wei, Y., & Li, L. (2022). Quantum tunneling effect on the surface enhanced Raman process in molecular systems. *Optics Express*, *30*(4), 4845. https://doi.org/10.1364/oe.450918

[73] Rohiman, A.; Anshori, I.; Surawijaya, A.; Idris, I.; Iskandar, F.; Abdullah, M. Study of Colloidal Gold Synthesis Using Turkevich Method; AIP, 2011.

[74] Nalbant Esenturk, E., & Hight Walker, A. R. (2009). Surface-enhanced Raman scattering spectroscopy via Gold Nanostars. *Journal of Raman Spectroscopy*, *40*(1), 86–91. https://doi.org/10.1002/jrs.2084

[75] Pei, Y., Wang, Z., Zong, S., & Cui, Y. (2013). Highly sensitive SERS-based immunoassay with simultaneous utilization of self-assembled substrates of gold nanostars and aggregates of Gold Nanostars. *Journal of Materials Chemistry B*, *1*(32), 3992. https://doi.org/10.1039/c3tb00519d

[76] Cui, S.-C., Tachikawa, T., Fujitsuka, M., & Majima, T. (2009). Solvent-polarity dependence of electron-transfer kinetics in a CdSe/ZnS Quantum Dot−Pyromellitimide Conjugate. *The Journal of Physical Chemistry C*, *114*(2), 1217–1225. https://doi.org/10.1021/jp909579j

[77] Gao, B., Lin, Y., Wei, S., Zeng, J., Liao, Y., Chen, L., Goldfeld, D., Wang, X., Luo, Y., Dong, Z., & Hou, J. (2011). Charge transfer and retention in directly coupled au-cdse nanohybrids. *Nano Research*, *5*(2), 88–98. https://doi.org/10.1007/s12274-011-0188-8

[78] Smitha, S. L., Gopchandran, K. G., Smijesh, N., & Philip, R. (2013). Size-dependent optical properties of AU nanorods. *Progress in Natural Science: Materials International*, *23*(1), 36–43. https://doi.org/10.1016/j.pnsc.2013.01.005

[79] Pei, L., Huang, Y., Li, C., Zhang, Y., Rasco, B. A., & Lai, K. (2014). Detection of triphenylmethane drugs in fish muscle by surface-enhanced Raman spectroscopy coupled with Au-Ag Core-shell nanoparticles. *Journal of Nanomaterials*, *2014*, 1–8. https://doi.org/10.1155/2014/730915

APPENDIX

Calculation of Au nanostar solution concentration:

1. Weight of gold taken

$$(0.01\ L) \times \left(0.001 \frac{mol}{L}\right) \times \left(196.96 \frac{g}{mol}\right) = 1.97 \times 10^{-3} g$$

2. Volume of gold taken

$$\frac{1.97 \times 10^{-3}\ g}{19.3\ g/cm^{-3}} = 1.02 \times 10^{-4}\ cm^3$$

3. Volume of single nanostar from FIB image

$$R = 67\ nm\ and\ \ r = 33.5\ nm$$

$$\frac{4\pi r^3}{3} = \frac{4\pi(33.5\ nm^3)}{3} = 1.57 \times 10^5\ nm^3$$

4. Number of particles in the solution

$$(1.02 \times 10^{-4} cm^3) \times (1.00 \times 10^{21}\ nm^3/cm^3) = 1.02 \times 10^{17}\ nm^3$$

$$\frac{1.02 \times 10^{17}\ nm^3}{1.57 \times 10^5\ nm^3} = 6.50 \times 10^{11}\ particles$$

$$\frac{(6.50 \times 10^{11}\ particles)}{10\ \mu L} = 6.50 \times 10^{10}\ \ particles/\mu L$$

UV-Vis of CdSe/ZnS QDs in toluene

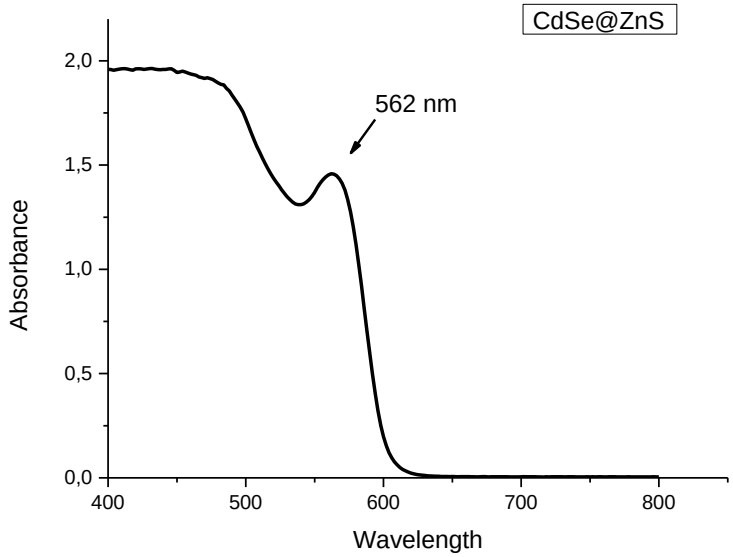

UV-Vis of Au nanostar 1

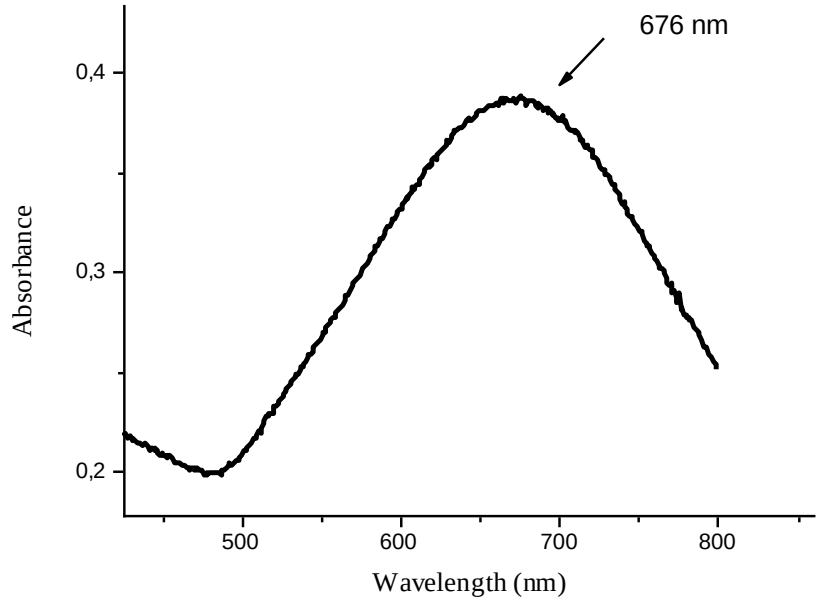

Box chart of SERS measurements with Au nanostar 1

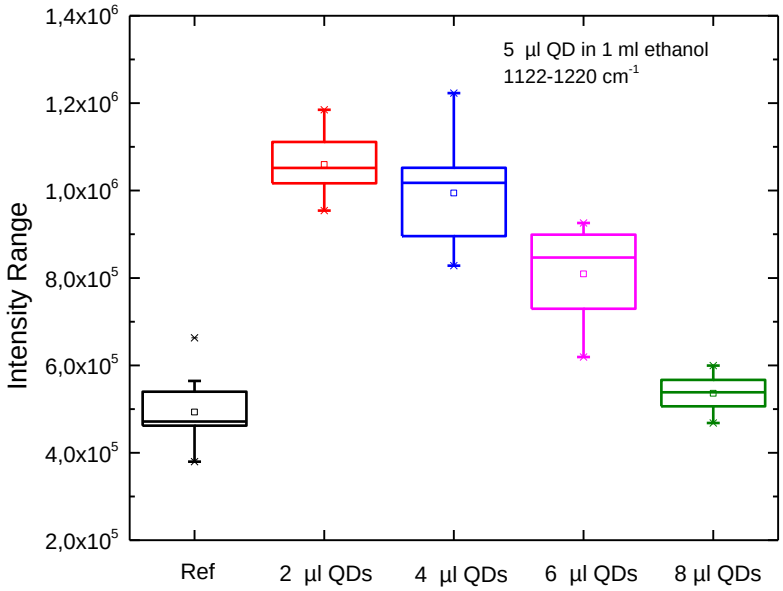

Solid state UV-Vis result of Au nanostar 1 and QDs mixture

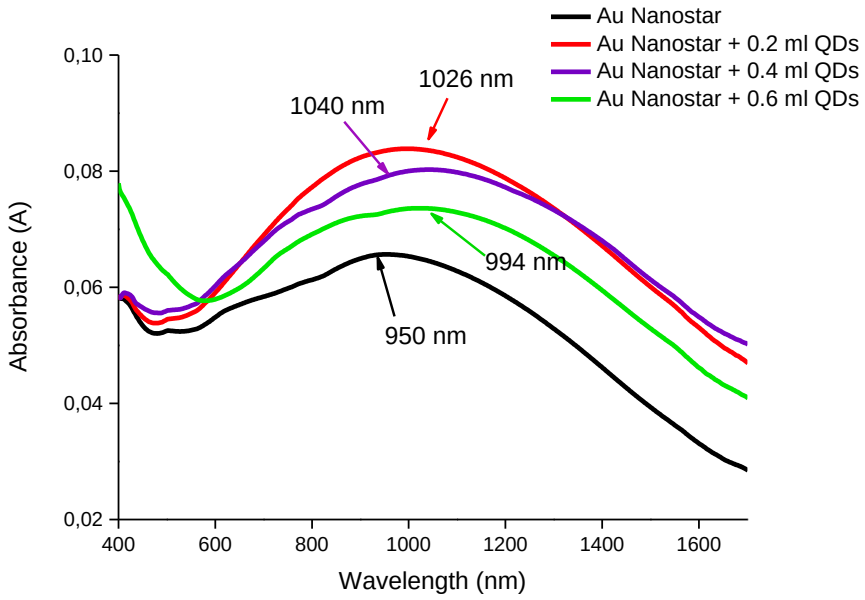

SERS samples were prepared and dried on Si-wafer to understand behavior of molecules in solid form. Solid state UV-Vis measurements were performed and box chart of SERS measurements associate with this study is given above.

UV-Vis of Au nanostar 2

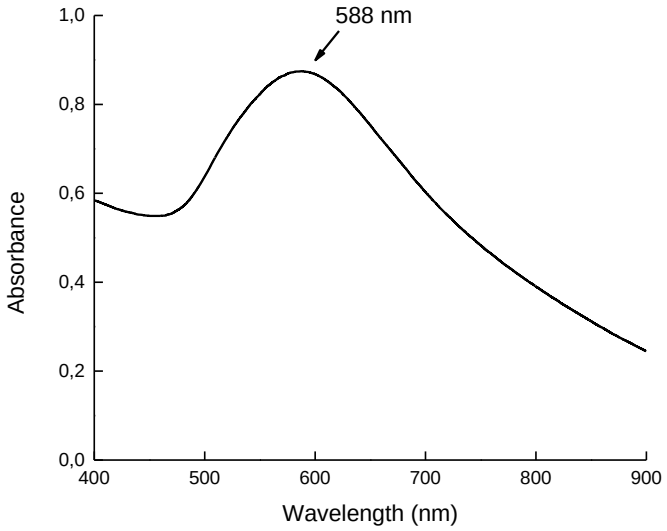

Box chart of SERS measurements with Au nanostar 2

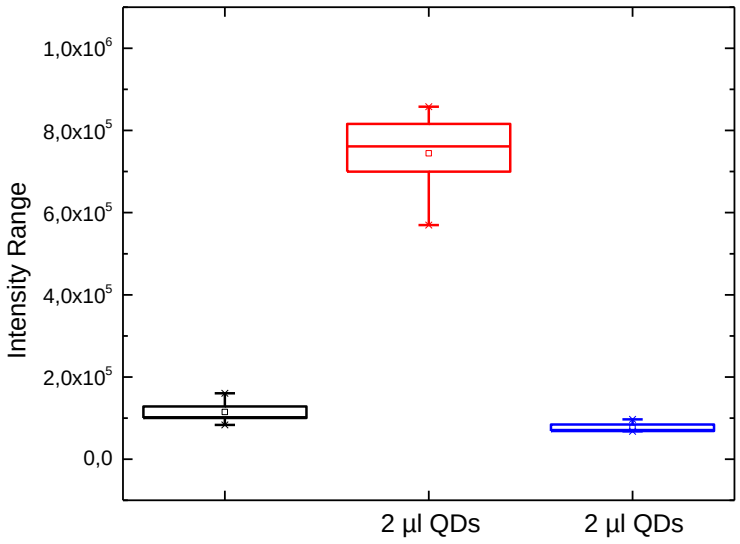

Enhancement Factor (EF) for presence of Au nanostar is calculated as follows:

Average size of Au nanostars is taken as 67 nm and 660 nm wavelength of laser spot size is 21 μm. N_{SERS} is calculated considering the extension of the near field to around 2 nm from the surface of the Au nanostars. Intensity of SERS is obtained from Figure 3.9. average intensity of Au nanostar and CV solution between 1584 and 1643 cm^{-1}. There are 7.7 x 10^4 Au nanostars on average at the laser spot area considering close-packed deposition of the Au nanostars on the Si wafer.

$$\frac{I_{SERS}}{I_{RAMAN}} \times \frac{N_{RAMAN}}{N_{SERS}} = Enhancement\ Factor\ (EF)$$

$I_{RAMAN} = 6.20\ x\ 10^4\ cts/s$ for 10^{-2} M

$$V_{Probe,Raman} = \frac{4\pi\ (10.5\ \mu m)(10.5\ \mu m)(21\ \mu m)}{3} = 9.69 \times 10^3\ \mu m^3$$

$$= 9.69\ \times 10^{-12}\ L$$

$N_{RAMAN} = C_{RAMAN} \times V_{PROBE}$

$N_{RAMAN} = 10^{-2}\ M\ \times 6.02 \times 10^{23}\ molecules/mol\ \times 9.69 \times 10^{-12} L$

$N_{RAMAN} = 5.83 \times 10^{10}\ molecules$

$$V_{Probe,SERS} = \frac{4\pi((34.5\ nm)^3 - (33.5\ nm)^3)}{3} = 1.45 \times 10^{-20}\ L$$

$V_{Probe,SERS} = 7.70 \times 10^4 \times 1.45\ \times 10^{-20} L = 1.11 \times 10^{-15}$

$N_{SERS} = 10^{-6} M \times 6.02 \times \frac{10^{23} molecules}{mol} \times 1.11 \times 10^{-15} L \times 10$ considering 10 layer of Au nanostar deposition.

$N_{SERS} = 6.68\ \times 10^3\ molecules$–

$I_{SERS} = 1.30 \times 10^5 cts/s$

$$EF = \frac{I_{SERS}}{I_{RAMAN}} \times \frac{N_{RAMAN}}{N_{SERS}} = \frac{1.30 \times 10^5 cts/s \times 5.83 \times 10^{10} molecules}{6.20 \times 10^4 \, cts/s \times 6.68 \times 10^3 \, molecules}$$

$$EF = 1.83 \times 10^7$$